

## Task 3.1

### Task Title

Geo-energy technologies

### Research Partners

Department of Mechanical and Process Engineering (D-MAVT) at ETHZ, Institute for Building Materials (IfB) at ETHZ, Lucerne University of Applied Sciences and Arts, University of Applied Sciences and Arts Western Switzerland (HES-SO), Laboratory for Hydraulic Machines (LMH) at EPFL

### Current Projects (presented on the following pages)

Affordable access to deep heat reservoirs: Flame-jet drilling

T. Meier, R. von Rohr

---

Numerical research on hydrothermal spallation drilling

F. Song, T. Meier, M. Schuler, R. von Rohr

---

Process conditions required for flame-jet drilling

D. Brkic, T. Meier, M. Kant, R. von Rohr

---

Investigation of the boundary conditions and process mechanisms of spallation drilling

A. Hobé, C. Madonna, M. Kant, J. P. Burg, R. von Rohr

---

Impact of polymers in oil-well cementing for geothermal wells

M. Palacios, R. K. Mishra, D. Sanz-Pont, R. J. Flatt

---

Tailor-Made Steels as Self-Protecting Corrosion Resistant Materials for Deep Geothermal Energy

A. Vallejo, U. Angst, B. Elsener

---

Detecting water through electric impedance measurements

G. Emery, G. Ganchinho, J. Moerschell

---

Deep Borehole Seismometer

J. Moerschell, C. Praplan, C. Cachelin, Y. Ravedoni

---

Development of numerical tools for heat transfer computations

D. Roos, L. Hanimann, L. Mangani, E. Casartelli

---

Analytical solution of the power production of a deep coaxial heat exchanger

R. Schnellman, P. Hardegger, H.R. Schneider

## Task Objectives

Five research groups are active in solving important technological problems in the application of geothermal energy. Without these technologies geothermal energy would not become economically competitive.

- **Innovative drilling technologies:** highly important to reduce the so far excessively high costs for drilling the deep wells
- **Cementitious grouts for bore holes in geothermal wells:** concrete has to be pumped for up to 5 km down and should remain fluid, so cement hydration must be delayed
- **Heat Exchangers for geothermal applications:** the efficiency of heat exchangers will determine economic feasibility
- **Sensors for harsh environments:** the main risk is that earth-quakes will be initiated, the sensors are very sensitive and monitor seismic activities during the drilling process.
- **Long term durable materials for geothermal plants:** long term operation of geothermal plants require durable materials without excessively high costs.

## Interaction Between the Partners – Synthesis

As the task group works on very different objectives, the research institutes exchange results in meetings at least two times a year. They have bilateral collaborations.

## Highlights 2015

- A new sensor concept for seismometers based on magnetic suspension of an inertial spherical mass is developed and validated; it is now on the prototype level. New is that the force feedback loops of the system are implemented digitally (Moerschell).
- Flame jet drilling is possible in lab-scale experiment. By increasing the compressing force on the rock sample, drilling is significantly improved.
- Numerical simulations can improve the understanding of the hydrothermal spallation drilling, provide more details than experiments (such as the temperature distribution in the whole field, velocity distribution, and also the effect of different structures), which will be helpful for designing and optimizing of the process.
- Combining conventional drilling technology with thermal spallation (flame jet drilling) could be a promising approach as about 3 – 4 times higher drilling velocities could be obtained (von Rohr).
- Hydration behavior of cements at high temperatures, especially the delay of initiation, could be rationalized by a physico-chemical model and experiments (Flatt).
- An high-temperature / high-pressure autoclave to study durability of metallic and inorganic materials in the geothermal brines is in the planning stage (Elsener)

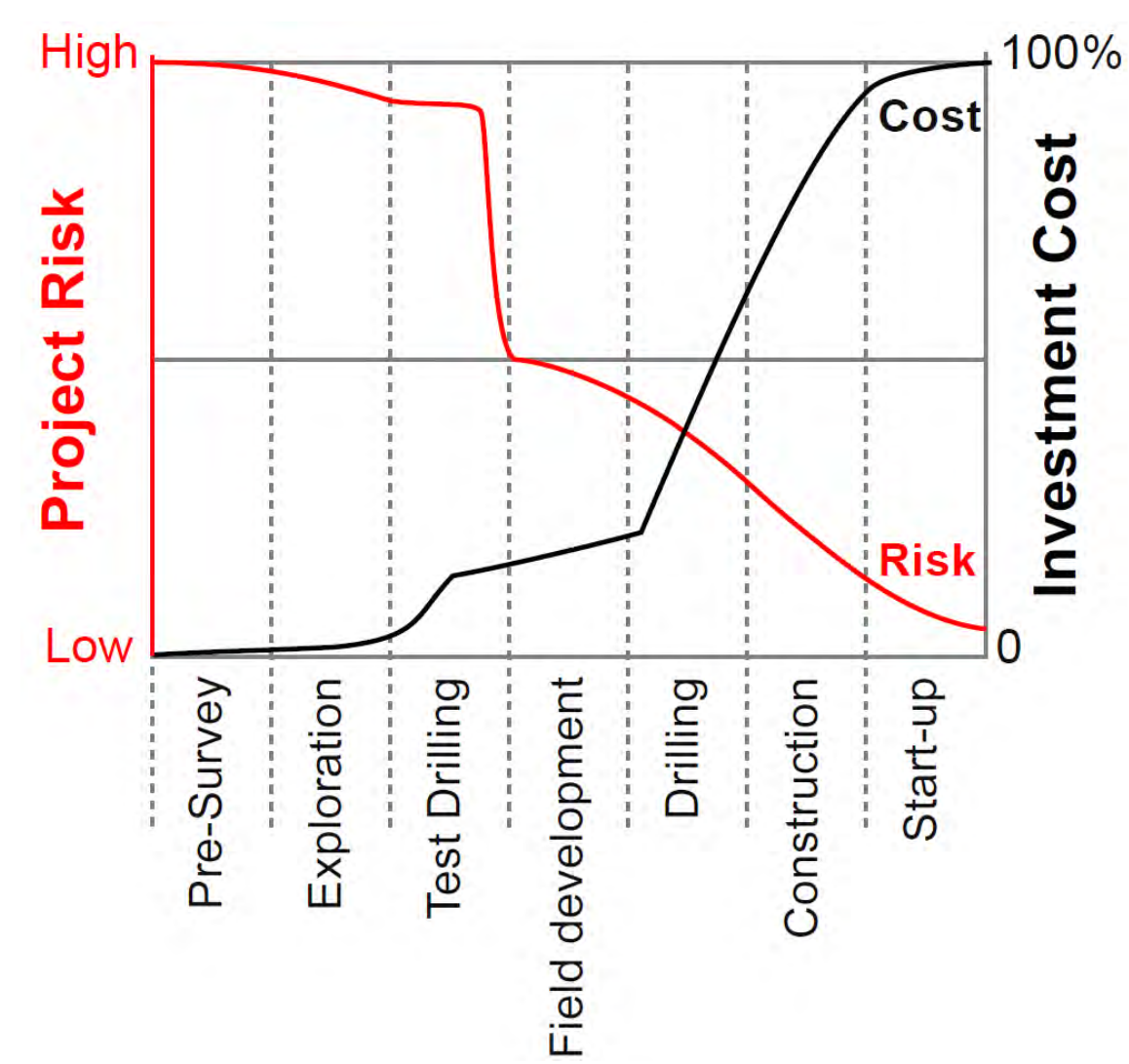
# Cost-effective access to deep energy reservoirs: flame-jet drilling

Thierry Meier, Dragana Brkic, Michael Kant, Feifei Song, Philipp Rudolf von Rohr

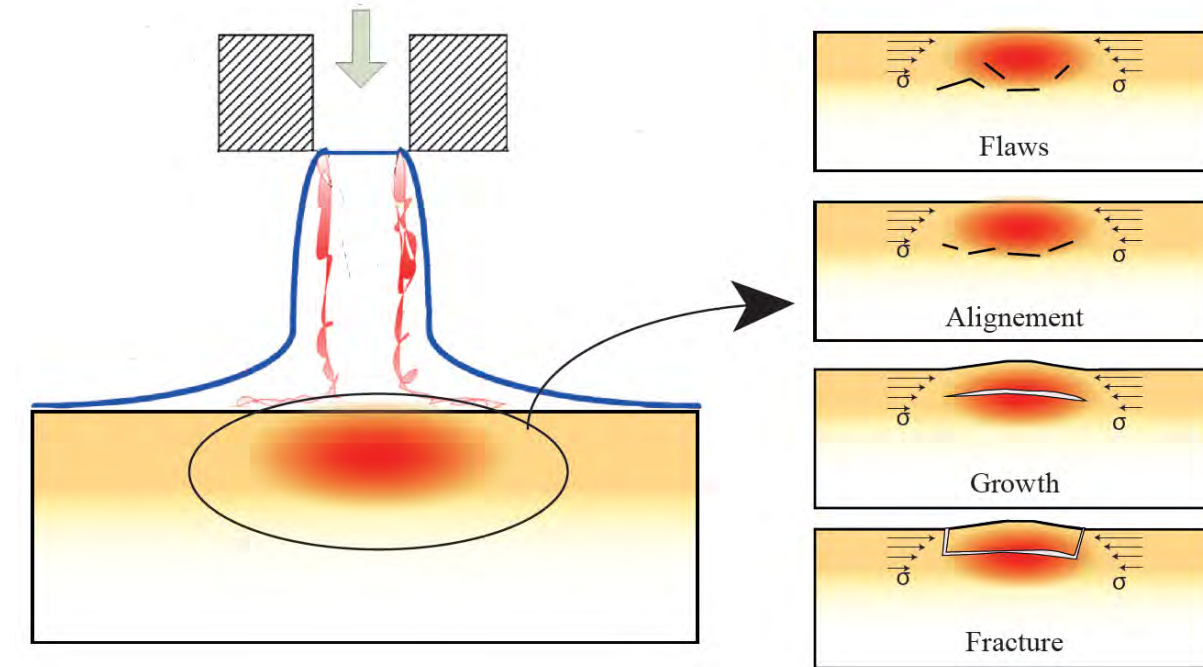
## Background and motivation

- 60% of the investment for a geothermal power plant concerns drilling
- 20% of the investment is spent with high risk

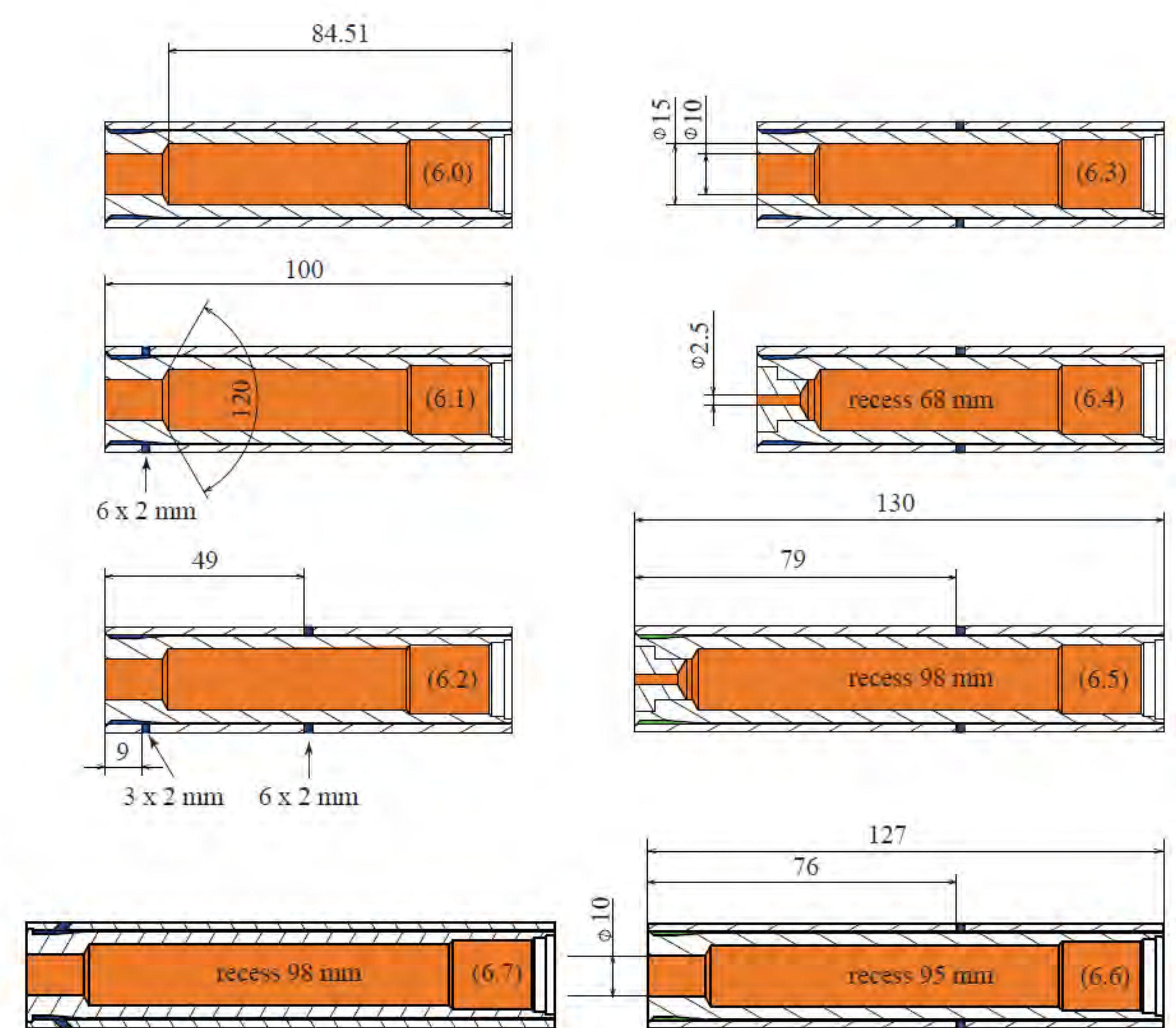
Source: The World Bank 002/2012



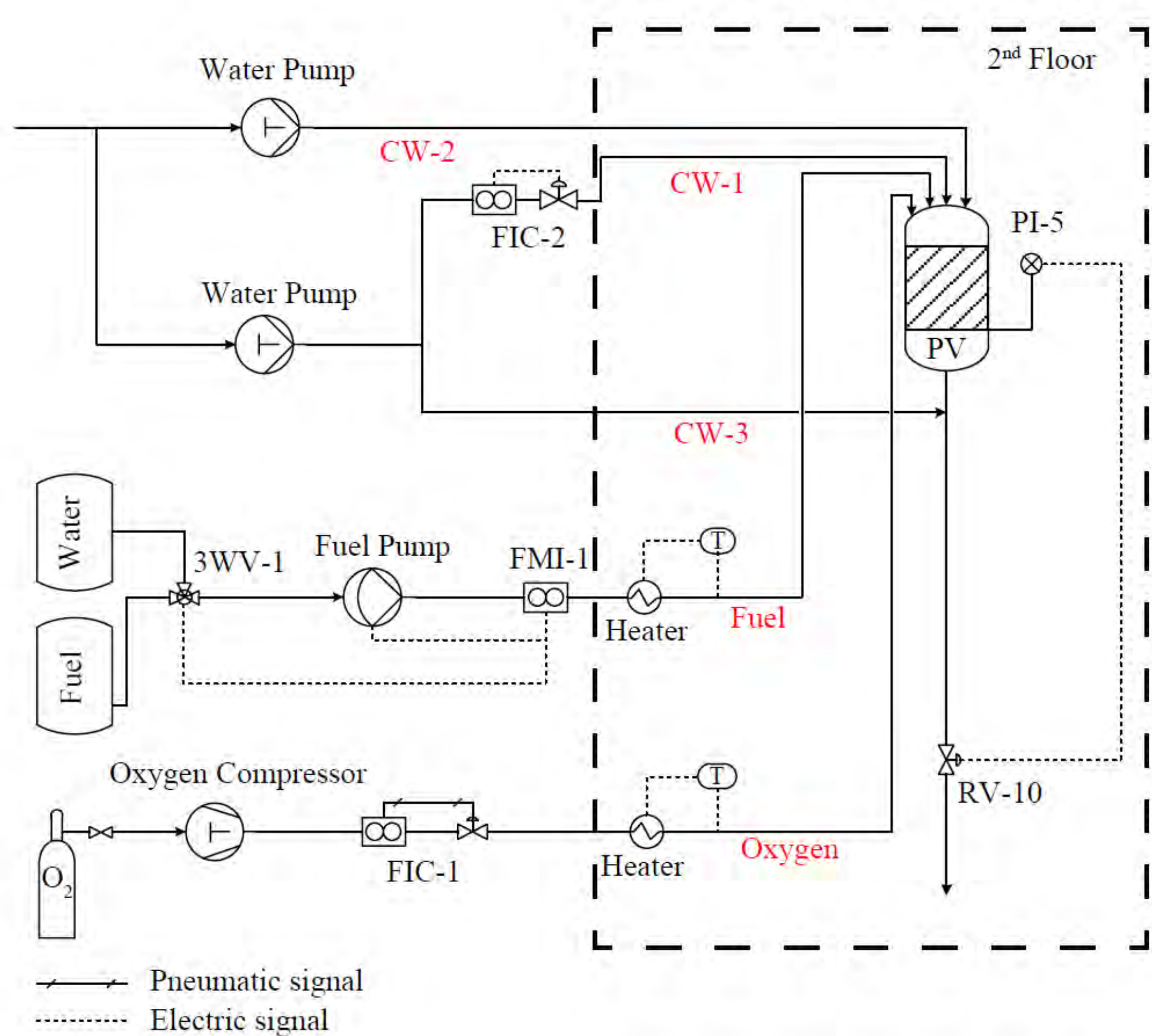
- The flame-jet induces an axisymmetric stress field
- Flaws extend due to the intense compression
- Exposed surface eventually flakes



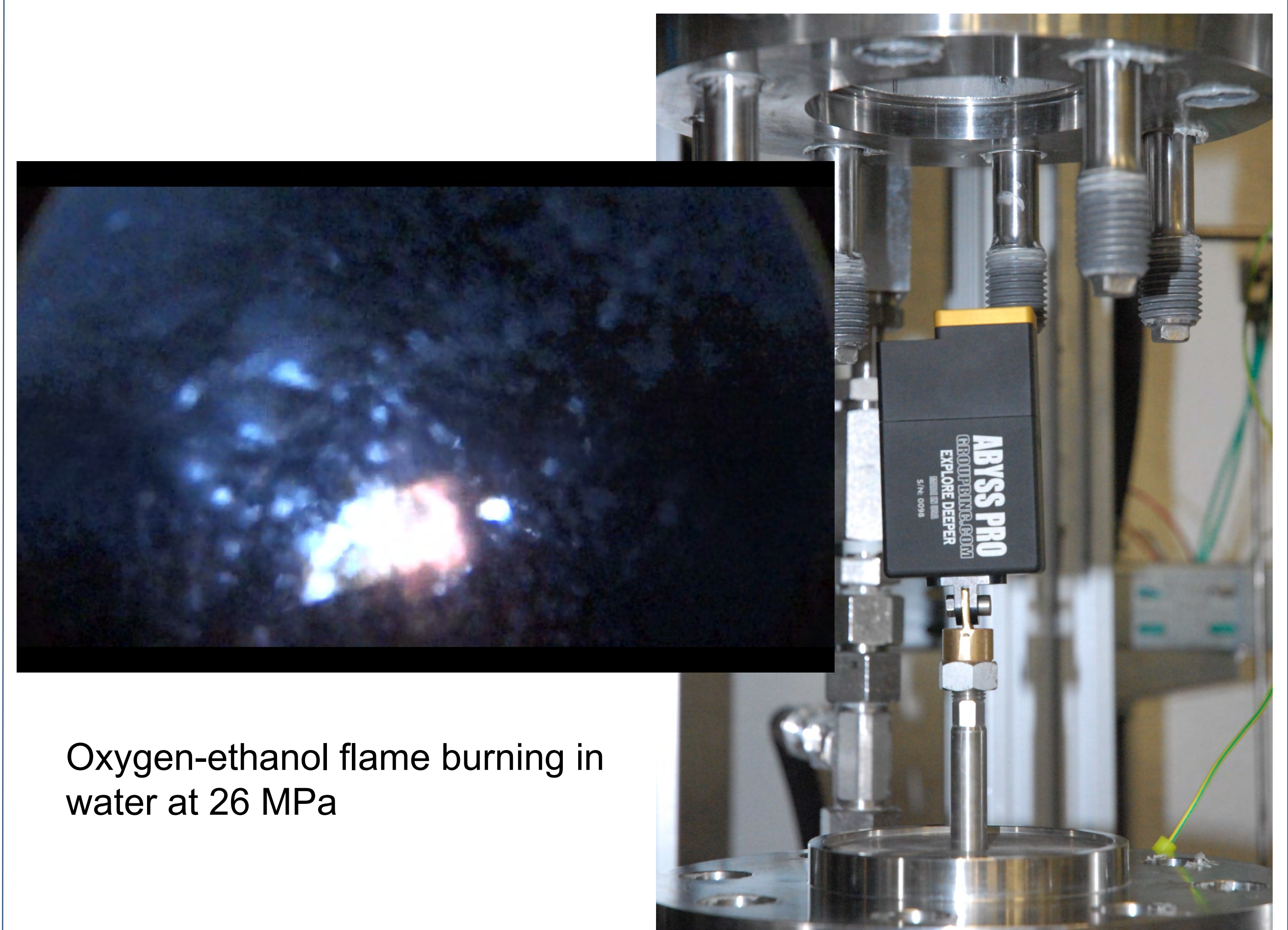
## 3. Flame-jet nozzle



## 1. Flame-jet drilling pilot facility

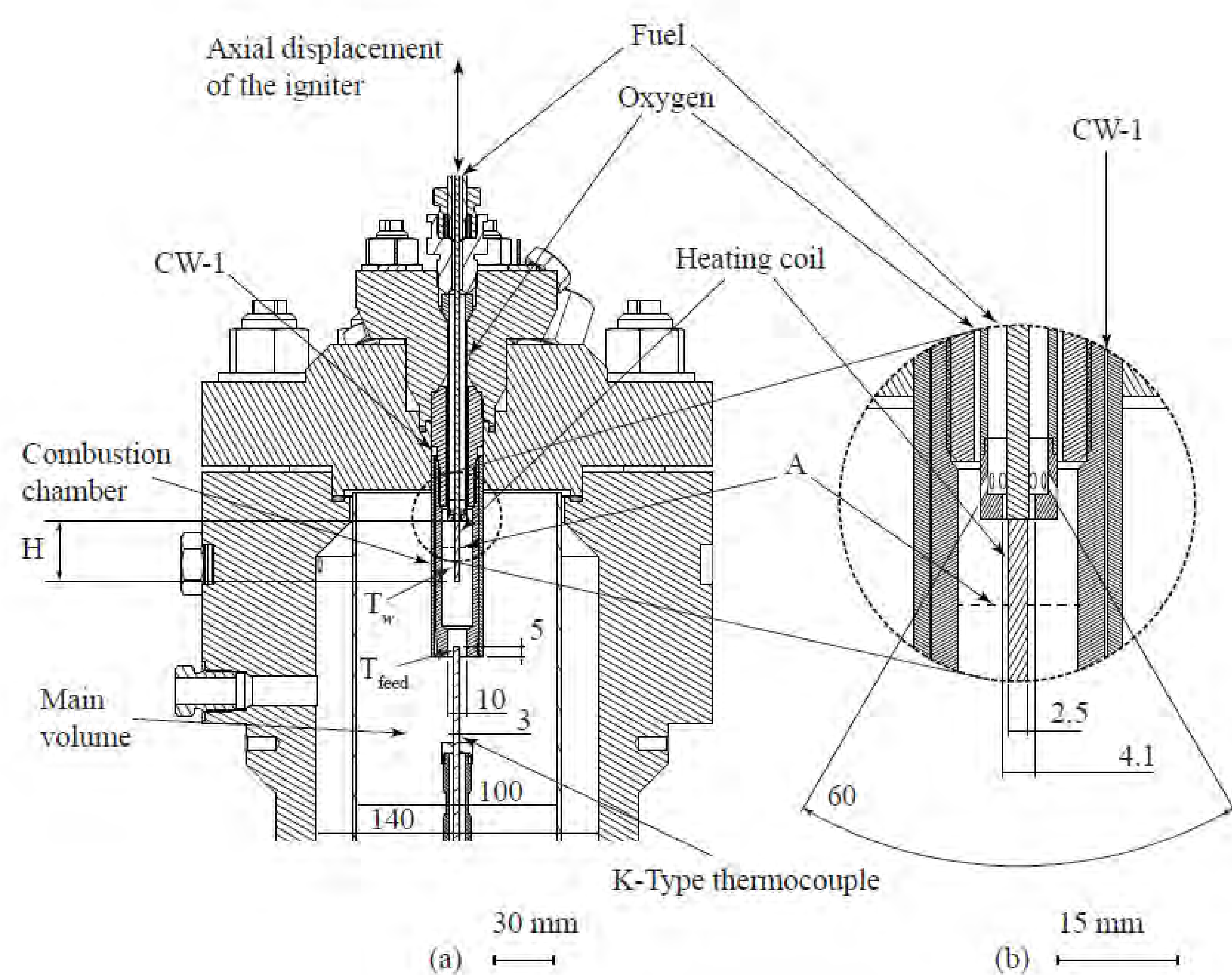


## 4. Flame ignition at 26 MPa

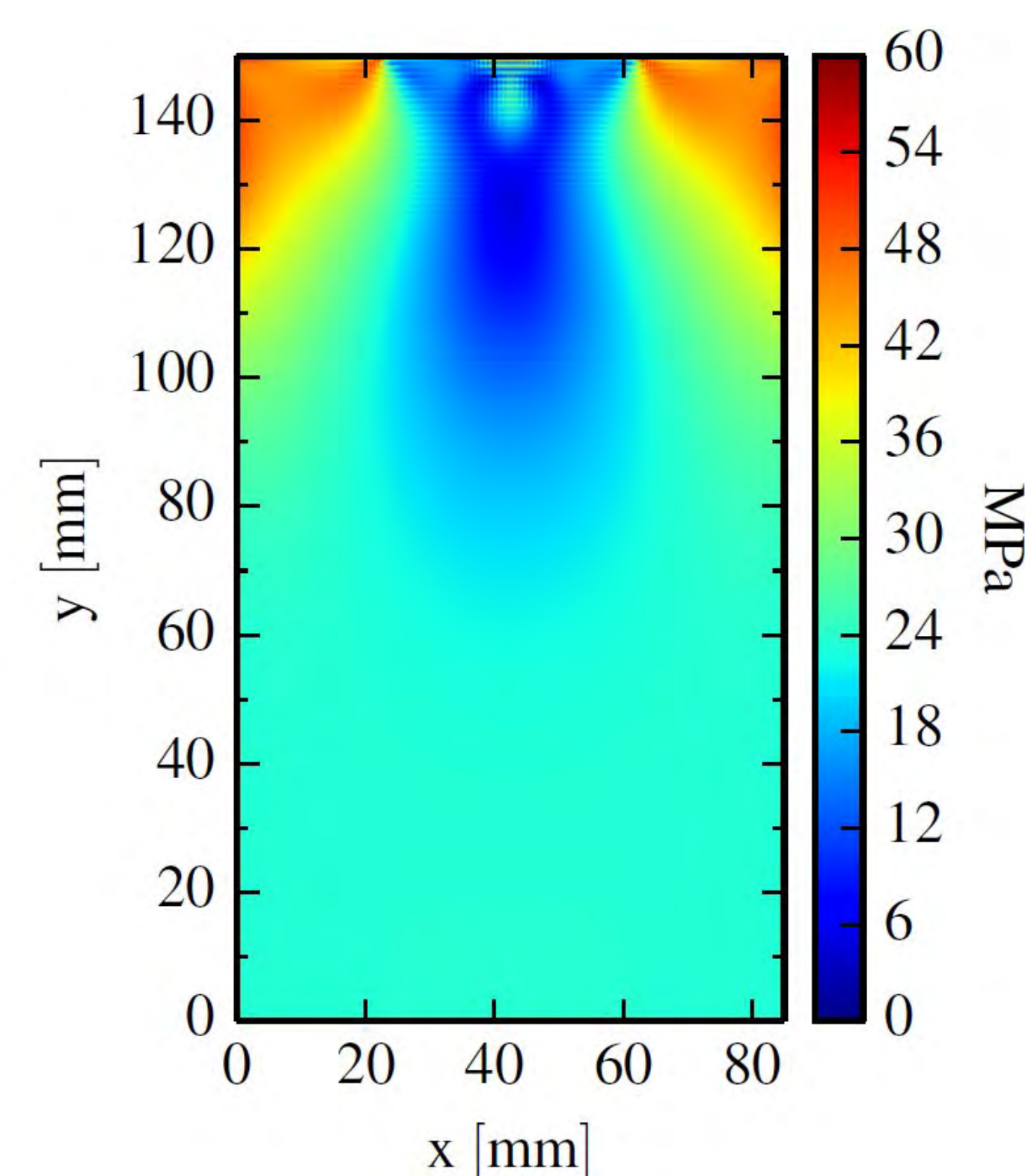


Oxygen-ethanol flame burning in water at 26 MPa

## 2. Pressure vessel and ignition system



## 5. Flame-jet drilling at 26 MPa



# Numerical research on hydrothermal spallation drilling

Feifei Song, Thierry Meier, Martin Schuler, Philipp Rudolf von Rohr

## 1. Introduction

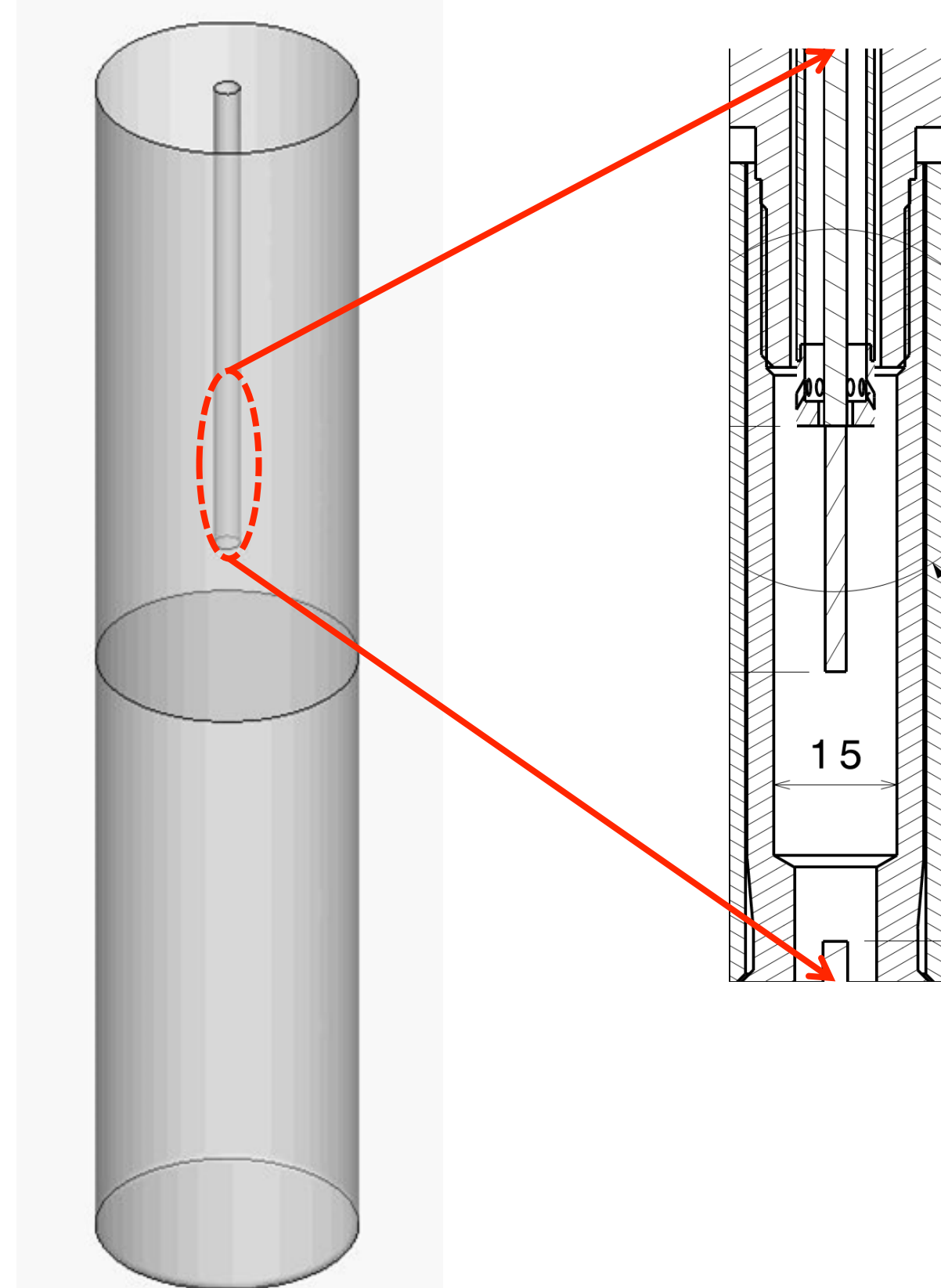
As a novel, contactless drilling technique, hydrothermal spallation drilling could reduce the drilling cost for deep drilling for hard rock and thus make geothermal energy more competitive.

Comparing with the experimental research, the numerical research has many benefits:

- Easier and cheaper to be carried out
- Give results which are hard to measure in experiments

## 2. Objective

With CFD (Computational Fluid Dynamics) simulations, we want to get a better understanding of the process of hydrothermal spallation drilling, such as the temperature distribution, heat flux to the rock, the rock stress, etc.

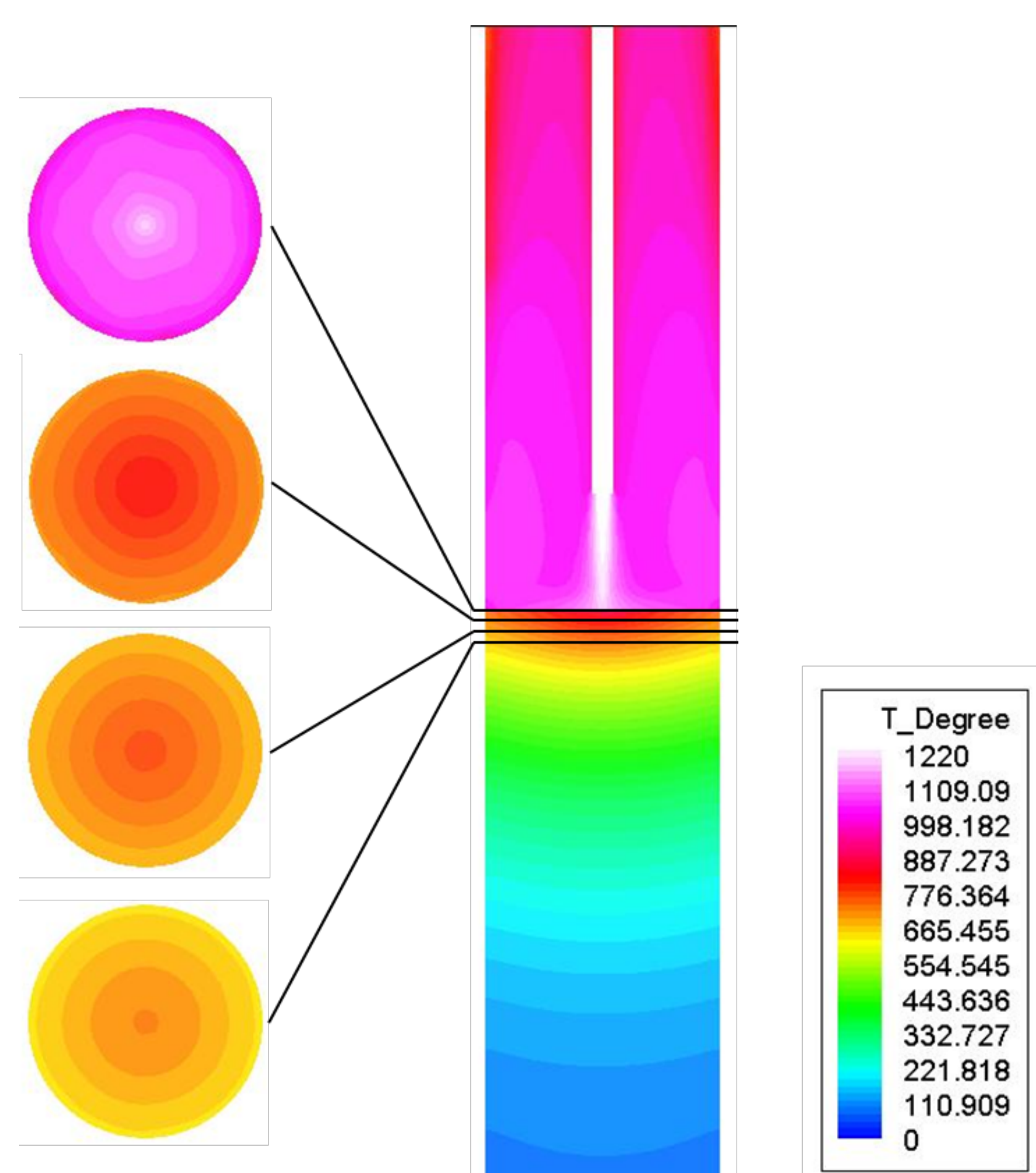


Schematic diagram of the simulation domain: combustion chamber and rock

The simulations focus on two parts:

1. Hydrothermal jet under supercritical condition
  - Include turbulence, species transfer, heat transfer, reaction and combustion
  - Aim to help designing and optimizing the drilling head
2. Spallation process without reaction
  - Heat transfer between the fluid and rock
  - Achieve distributions in the fluid and rock
  - Moving boundary to simulate the spallation process

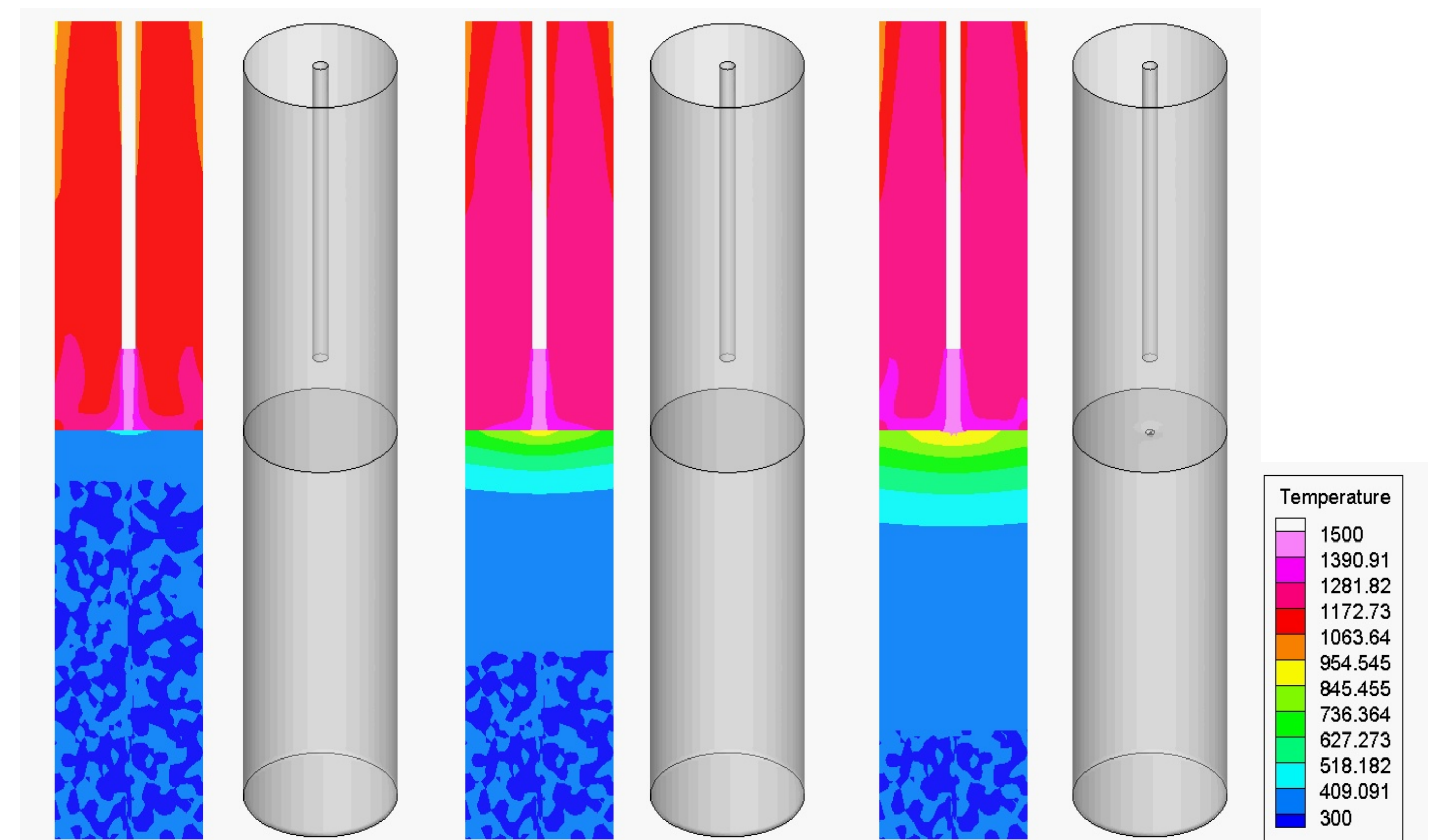
## 3. Temperature distribution without drilling



Temperature distribution (°C) in the fluid (upper part) and rock (lower part) when no drilling happens and no consideration of the structure of drilling head

## 4. Preliminary results of spallation process

As a preliminary try, for simplicity, here the fluid is simplified as a kind of hot air, and the structure of the drilling head is not considered. At the same time, we assume the spallation happens only when temperature of rock surface is above some threshold value.



Temperature distribution (K) and drilling process at different time: 0s, 20s, 40s, 60s, 80s, 100s

## 5. Outlook

1. Simulations around the drilling head
  - With detail structure of the drilling head
  - With supercritical condition
2. Spallation process
  - More reasonable rule to determine whether spallation happens
  - Using temperature from the drilling head simulations
  - With supercritical condition
3. Validate by experimental data

## 6. Conclusions

CFD simulations can improve our understanding of the hydrothermal spallation drilling and give us more details than experiments (such as the temperature distribution in the whole field, velocity distribution, and also the effect of different structures), which will be helpful for the designing and optimizing.

# Process conditions required for flame-jet drilling

Dragana Brkic (brkicd@ethz.ch), Thierry Meier, Michael Kant, Philipp Rudolf von Rohr



## Thermal spallation as a drilling mechanism

Exploitation of geothermal energy requires drilling deep wells through a hard crystalline rock to reach the regions of sufficiently high temperatures beneath the Earth's surface. For accomplishing this task in an energy-efficient and cost-effective way existing drilling methods should be improved, or a new one developed. Thermal spallation drilling presents one method that offers a potential for substantial cost reduction [1]. It is based on inducing a temperature gradient within the surface layer of the material (rock) by the heat transferred from an impinging flame jet. This temperature gradient is reflected by the thermal stresses eventually leading to the detachment of disc-like fragments (spalls) from the surface [2,3].

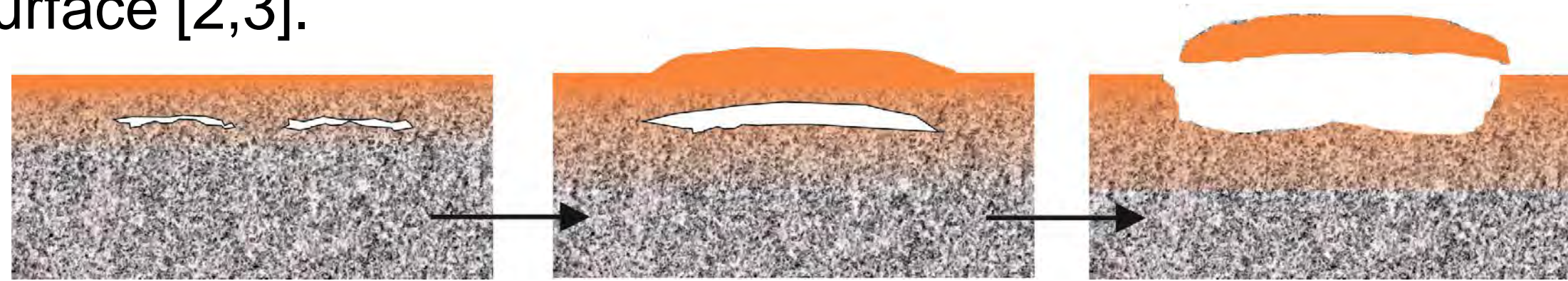


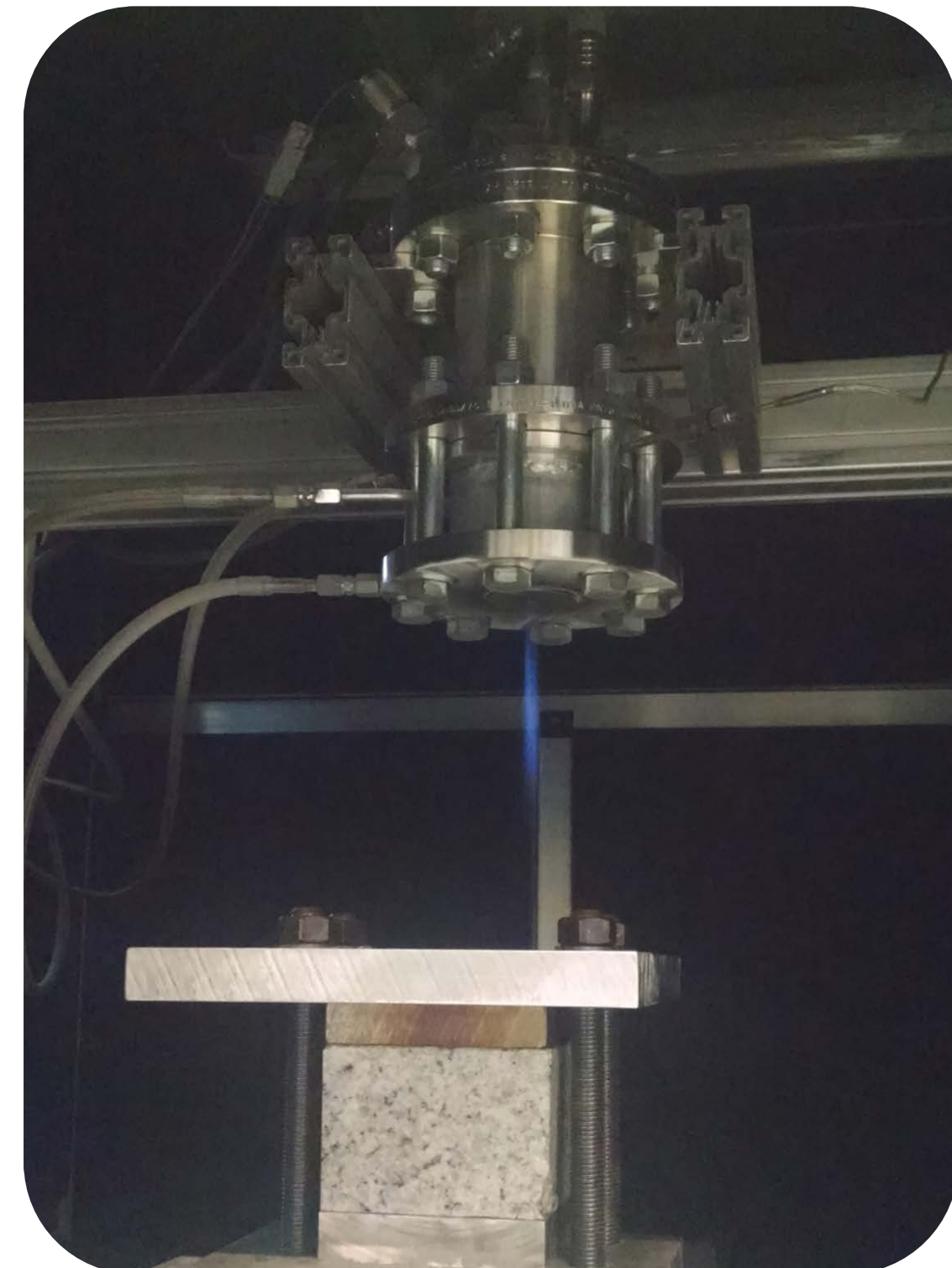
Fig. 1 Thermal spallation mechanism – expansion of the upper layer and its detachment from the rock surface [4]

## Drilling setup - description

Setup	Hydrothermal Closed system No optical access	Ambient Opened system With optical access
Surrounding	Supercritical water	Air
Pressure	260 bar	1 bar



Fig. 2 a) High pressure drilling setup



b) Ambient drilling setup

## Required conditions for successful thermal spallation

The transferred heat is an important parameter for elucidating thermal spallation mechanism and it can be calculated by Eq. 1:

$$\dot{q} = h (T_{flame} - T_{surface}) \quad (1)$$

where the flame temperature ( $T_{flame}$ ) can be measured by a thermocouple and the heat transfer coefficient ( $h$ ) can be calculated from the measured heat flux with a heat flux sensor, respectively.

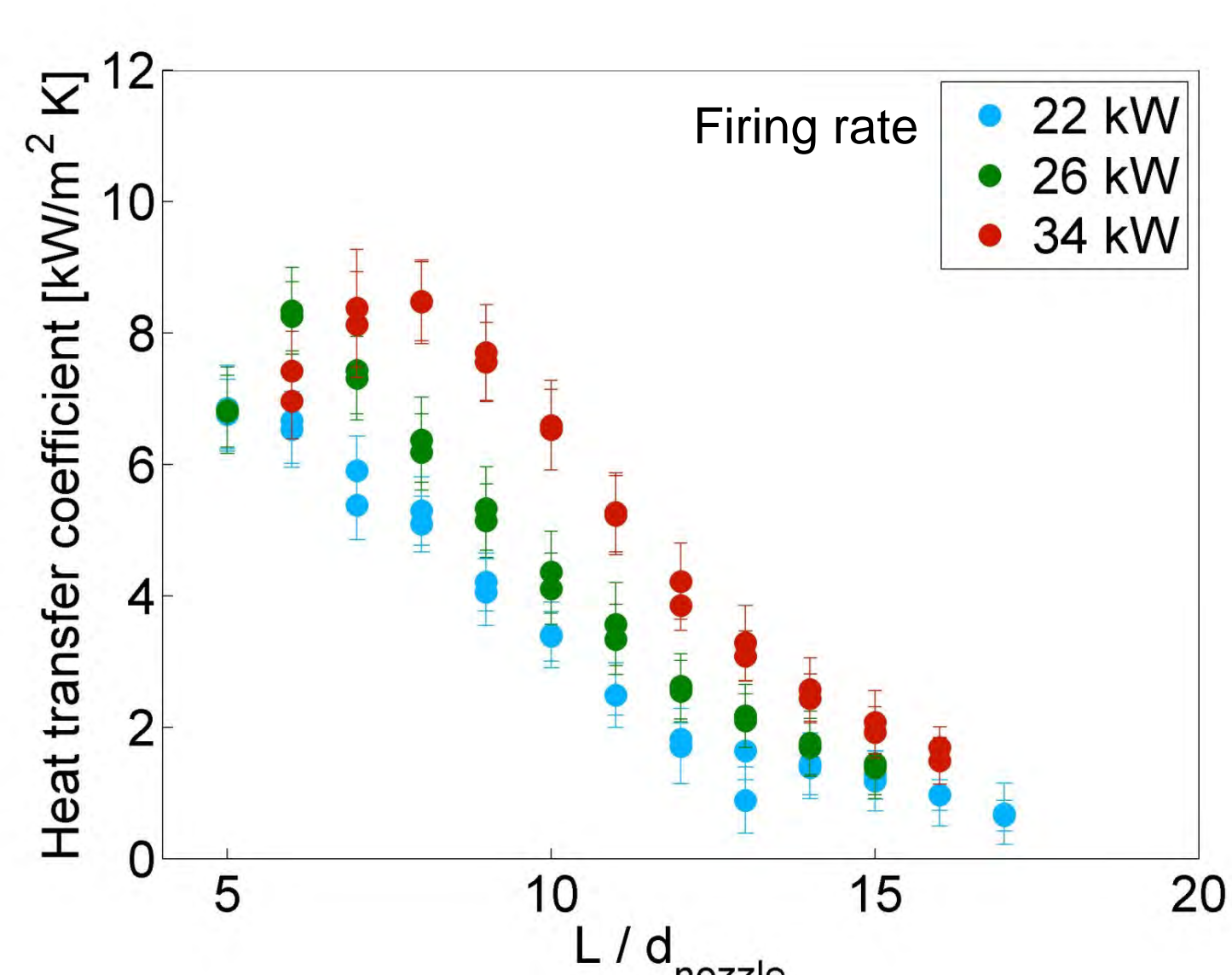


Fig. 3 Heat transfer study from the impinging flame jet to a heat flux sensor

## Calorimeter – heat flux sensor

In calorimetric heat flux measurements, the heat transferred from the impinging flame jet to the surface of the sensor is calculated by Eq. 2:

$$\dot{q} = \dot{m}_{water} \Delta T_{water} \quad (2)$$

where  $\dot{m}_{water}$  presents the mass flow and  $\Delta T_{water}$  the temperature rise of the cooling water stream flowing under the surface of the calorimeter.

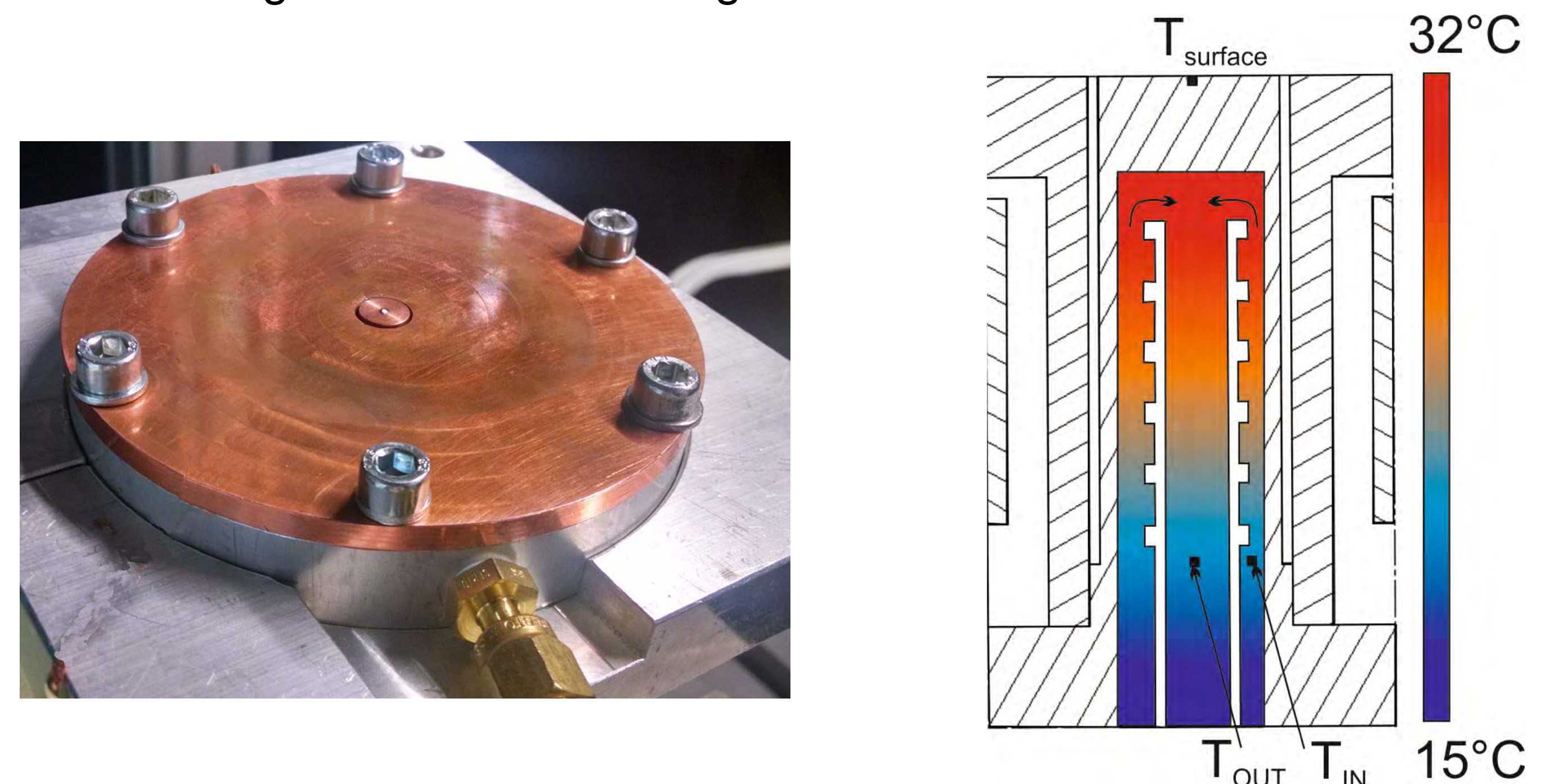


Fig. 4 Calorimeter – heat flux sensor

Fig. 5 Cross section of the sensor

## Compression of the rock sample- improved flame jet drilling

In order to reduce the thermal expansion of the rock sample and cracking over its whole volume during the experiment, the rock sample was compressed between two plates (Fig 6 a). It is believed that described system simulates the underground conditions and increases the compressive stress in the material. As a result, the flame jet drilling has been significantly improved.

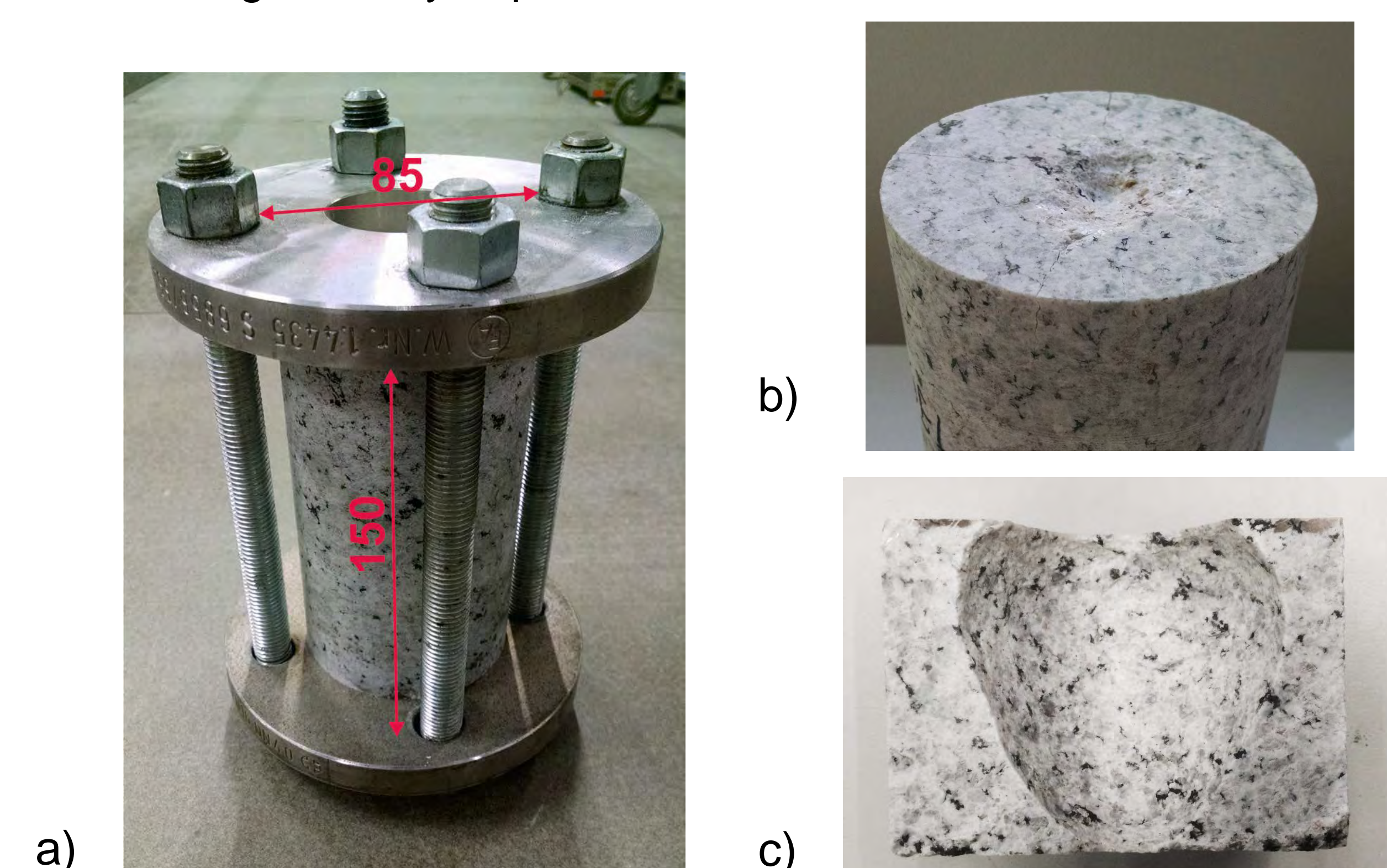


Fig. 6 a) compressed rock sample, b) results of spallation without compression b) with compression

## Conclusion

Flame jet drilling is possible in lab-scale experiment. There is a potential to discover the influence of the heat transfer coefficient on thermal spallation. Also, by increasing the compressing force on the rock sample drilling is significantly improved.

## References

- [1] J. W. Tester, et al., Proc. World Geotherm. Congr. Florence, Italy, 1995
- [2] R. M. Rauenzahn, Analysis of Rock Mechanics and Gas Dynamics of Flame-Jet Thermal Spallation Drilling, Ph.D. thesis, Massachusetts Institute of Technology, 1986
- [3] M. A. Wilkinson, J. W. Tester, *Rock Mech. Rock Eng.* 26:29-62, 1993
- [4] F. W. Preston, H. E. White, *Journal of the American Ceramic Society*, 17:137-144, 1934.

# Investigation of the boundary conditions and process mechanisms of spallation drilling

M. Kant, C. Madonna, A. Hobé, J.-P. Burg, P. Rudolf von Rohr

## 1. Introduction

Spallation Drilling is a contactless drilling technology for geothermal or petrological deep drilling operations. It is based on the effect that certain rocks locally disintegrate into small fragments, if they are suddenly exposed to high thermal loads, e.g. flame jets. In order to enhance the understanding of the process, the fluid-side conditions and the mechanisms leading to the spallation effect have to be understood.

## 2. Fluid-side operating conditions for spallation

### Important Parameters:

for a successful initiation of spallation [1,2]

- Heat transfer coefficient  $h_{fl}$
- Surface Temperature  $\vartheta_{SP}$

### Limitations:

applicable boundary conditions

- Upper limit: Melting of the minerals inhibits spallation  
→ Material parameter (ca. 1000°C)
- Lower limit: Minimal conditions where spallation can be initiated  
→ Experimental measurements required

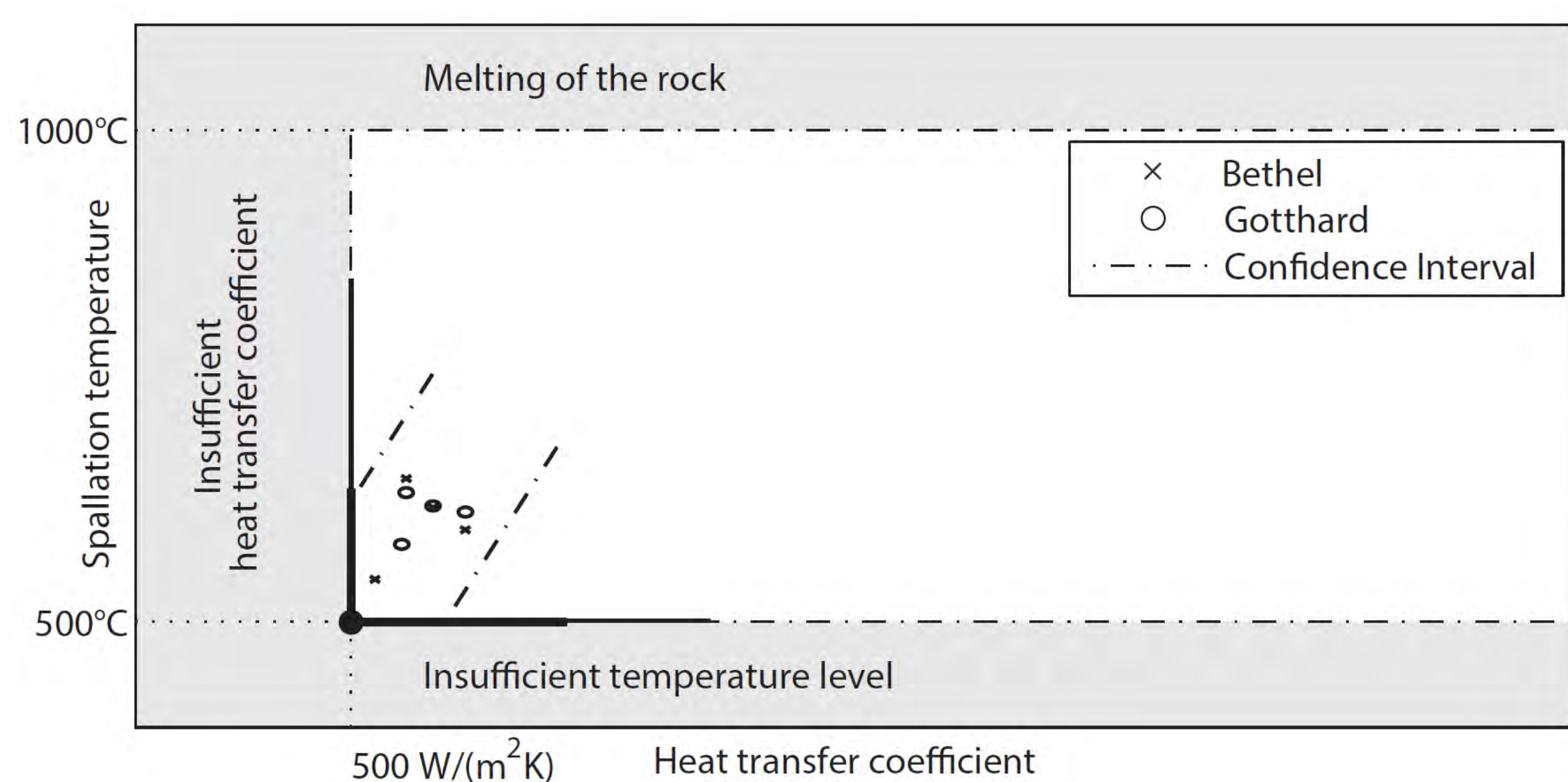


Fig. 1: Applicable operating conditions for thermal spallation drilling with experimental measurements for the determination of the minimal applicable boundary conditions

## 3. Influence of fluids on the spallation mechanism

Figure 2 shows the current proposed spallation mechanism:

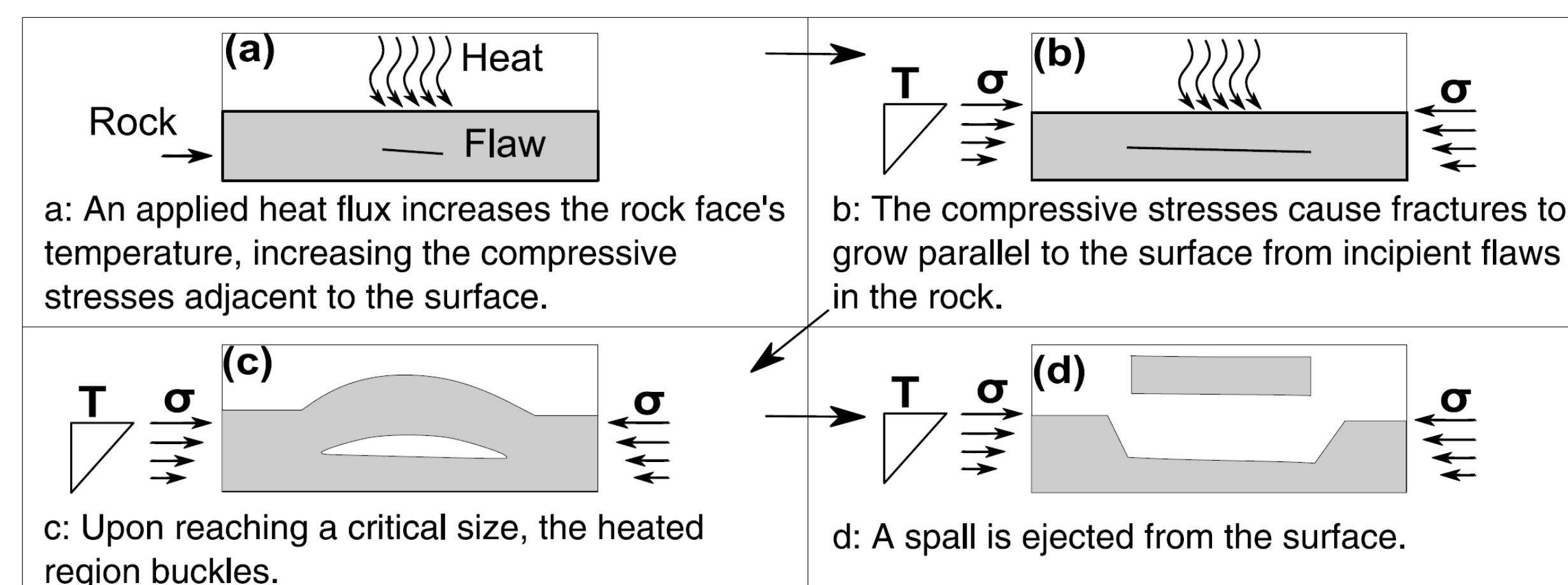


Fig. 2: Spallation model by Preston and White[1], modified from Walsh and Lomov [4]

### Scanning Electron Microscopy

- Investigation of fragments created during thermal spallation
- Biotite is deformed after spallation
- Fractures originate at and connect biotite crystals  
→ additional, positive effect on the spallation mechanism

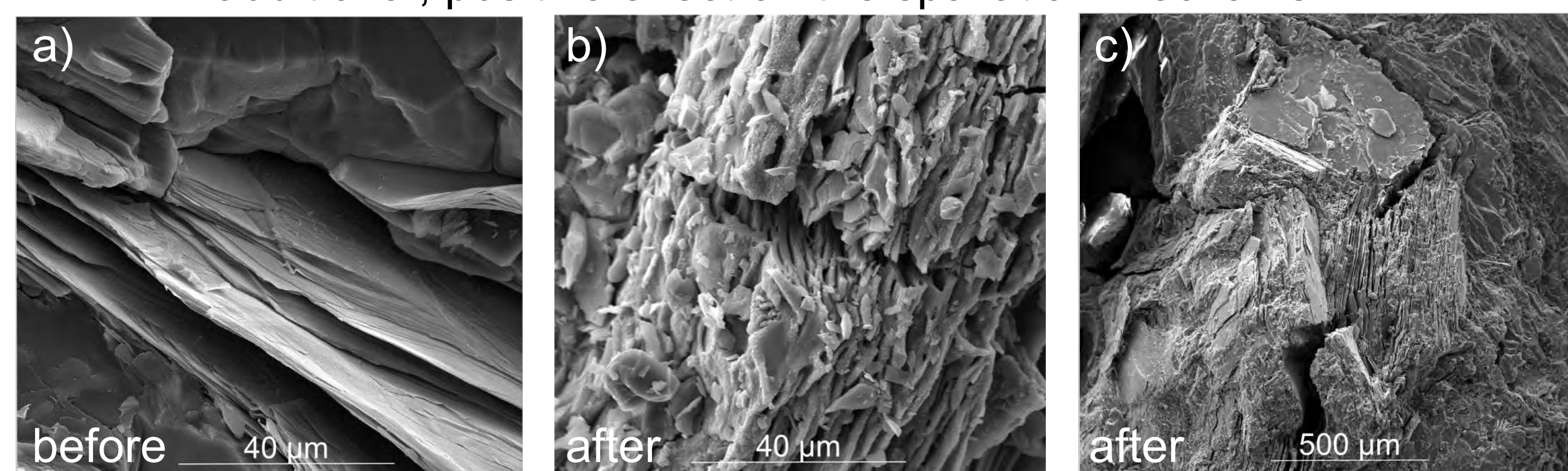


Fig. 3: SEM pictures: a) before spallation, b),c) after spallation

### Computer modelling

Simulations of the thermal stresses show a significant increase in the stresses, if fluid release by hydrous minerals are considered [3]:

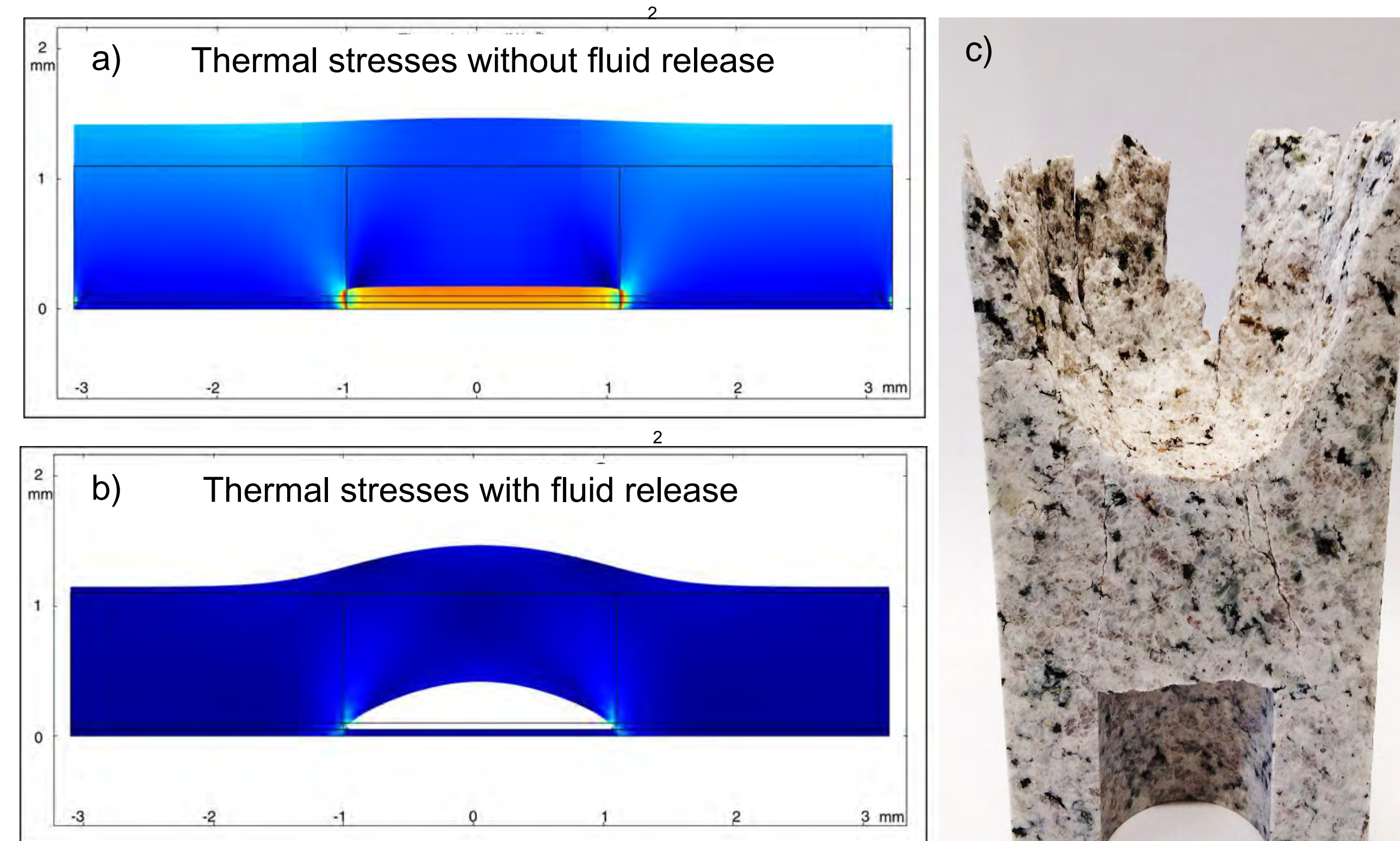


Fig. 4: a) Differential expansion of quartz and biotite. b) Same model with water replacing part of the biotite c) rock sample after the spallation experiment

### Fluid releasing thermal spallation

Figure 5 shows the proposed additional mechanism for thermal spallation of rocks containing hydrous minerals.

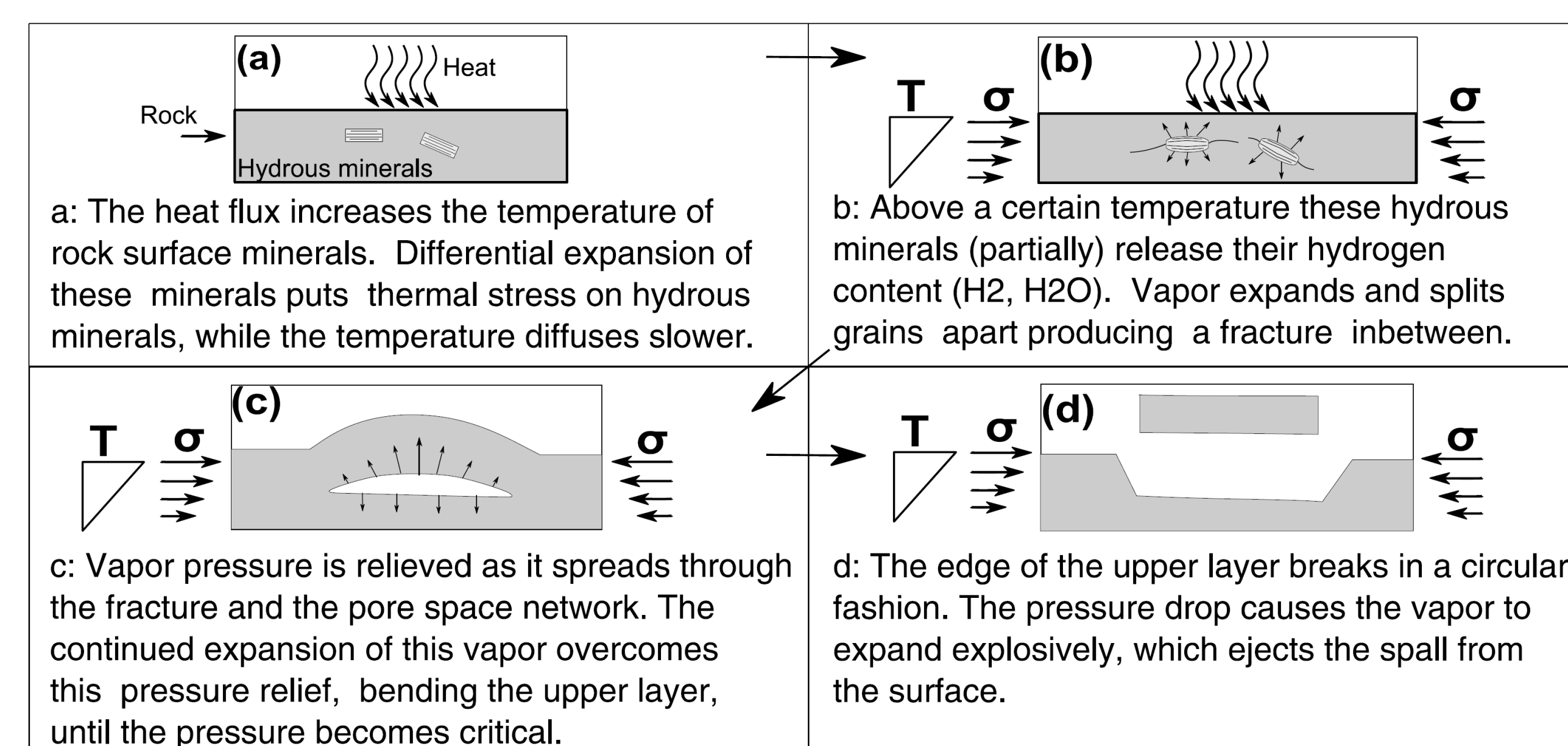


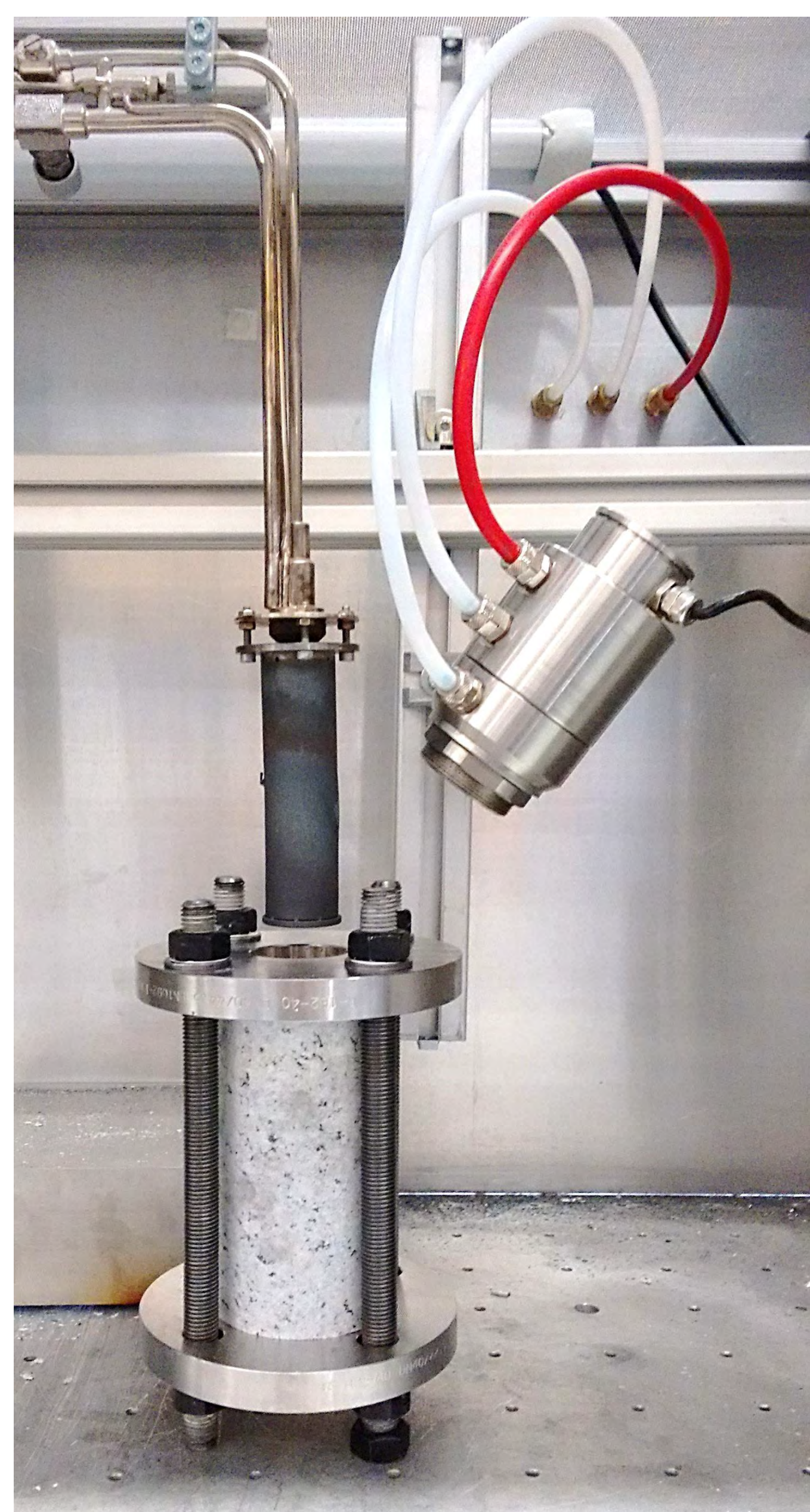
Fig. 5: Proposed additional thermal spallation mechanism (modified from Walsh and Lomov [4])

### References:

1. Wilkinson, M. A.; Tester, J. W. (1993): Experimental measurement of surface temperatures during flame-jet induced thermal spallation. In: *Rock Mech Rock Eng* 26 (1), S. 29-62. DOI: 10.1007/BF01019868.
2. Preston, F. W.; White, H. E. (1934): Observations on spalling. In: *Journal of American Ceramic Society* 17 (1-12), S. 137-144. DOI: 10.1111/j.1151-2916.1934.tb19296.x.
3. Rimsaite, J. (1970): Structural formulae of oxidized and hydroxyl-deficient micas and decomposition of the hydroxyl group. *Contributions to Mineralogy and Petrology*, 25, 225-240.
4. Walsh, Stuart D.C.; Lomov, Ilya N. (2013): Micromechanical modeling of thermal spallation in granitic rock. In: *International Journal of Heat and Mass Transfer* 65, S. 366-373. DOI: 10.1016/j.ijheatmasstransfer.2013.05.043.

### Acknowledgements:

Swiss Federal Office of Energy, Francesca Forni, Dr. Daniela Hunziker, Dr. Karsten Kunze, Dr. Peter Brack, Peter Nievergelt, Martin Schuler, Thierry Meier, Dragana Brkic



### Experimental overview:

#### Setup:

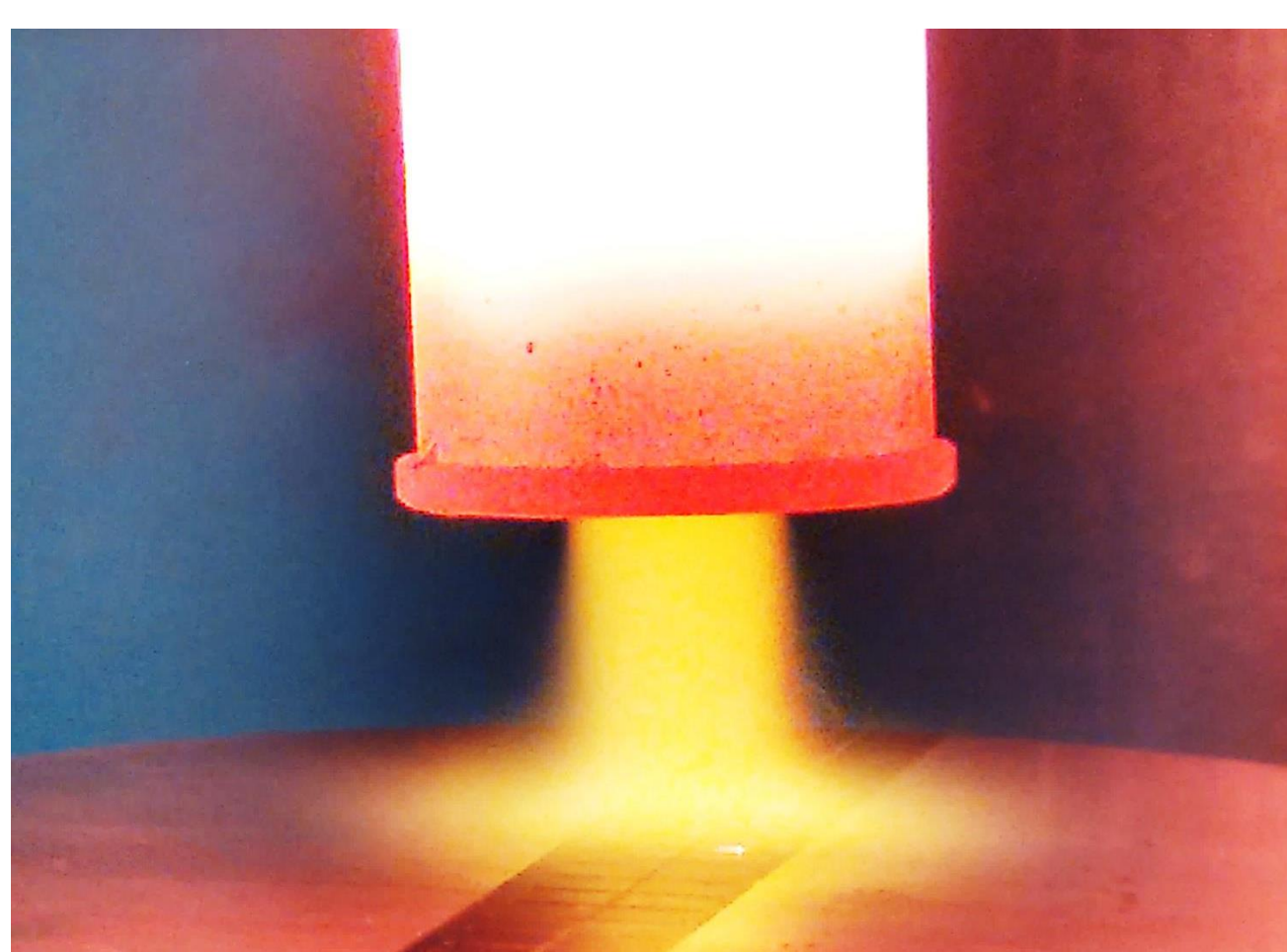
- Flame: Oxygen-Air-Methane
- Power: 20kW
- Temperatures: 2500 °C

#### Temperature Measurements:

- High-speed Pyrometer
- Sampling rate: 1000 Hz
- Emissivity calibration required

#### Heat transfer measurement:

- Commercial sensor



# Tailor-Made Steels as Self-Protecting Corrosion Resistant Materials for Deep Geothermal Energy

A. Vallejo, U. Angst, B. Elsener \*

## 1. Introduction

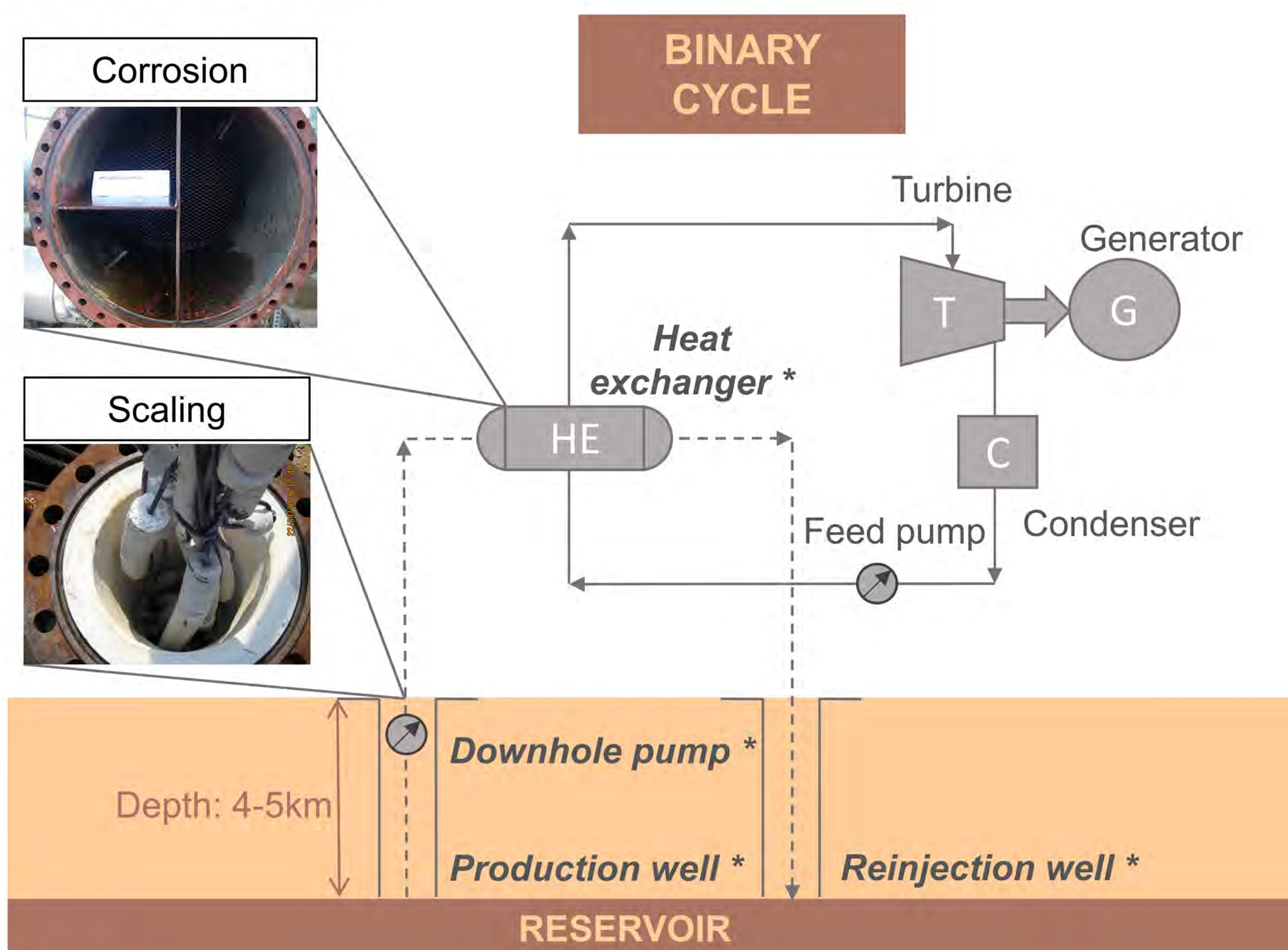
Deep geothermal energy systems are not exempt of technical problems. Corrosion and scaling issues represent major hazards for the reliable and long-term operation of geothermal power plants. Whereas corrosion products are the result of electrochemical reactions of the material with the environment, scaling is due to the precipitation of solids dissolved in the aqueous solution.

In deep geothermal systems, commonly used steels (i.e. carbon and low-alloy steels and stainless steels) are mainly subject to uniform corrosion, pitting corrosion, or stress corrosion cracking. On the other hand, scaling products (e.g. silica, calcite) form as the solubility decreases, due to temperature or pressure changes. Both phenomena can be regarded as correlated processes, since scaling products may deposit from brine on top of the corrosion product layer. In literature, there exist some controversy on whether this scaling is beneficial or not for the further protection of the metal.

This project proposes a fundamentally new approach to extend the service life of deep geothermal facilities and ensure safe, cost-effective, and maintenance-free long term operation. The expected outputs are a detailed understanding of the corrosion and scaling mechanisms in binary geothermal systems and the characterization of various metallic materials in these environments.

## 2. Binary Geothermal Power Plants

Main technical problems for the reliable and long-term operation of binary power plants:



\* Components exposed to the geothermal fluid

## 3. Influencing Factors

Geothermal environments are aggressive and exhibit reducing conditions. The main influencing agents are identified as follows:

- Environment:  $Cl^-$ ,  $H^+$ ,  $CO_2$ ,  $H_2S$ , high temperature
- Operational conditions: shut-down ( $O_2$  entrance), pressure change

Many research questions are still unresolved:

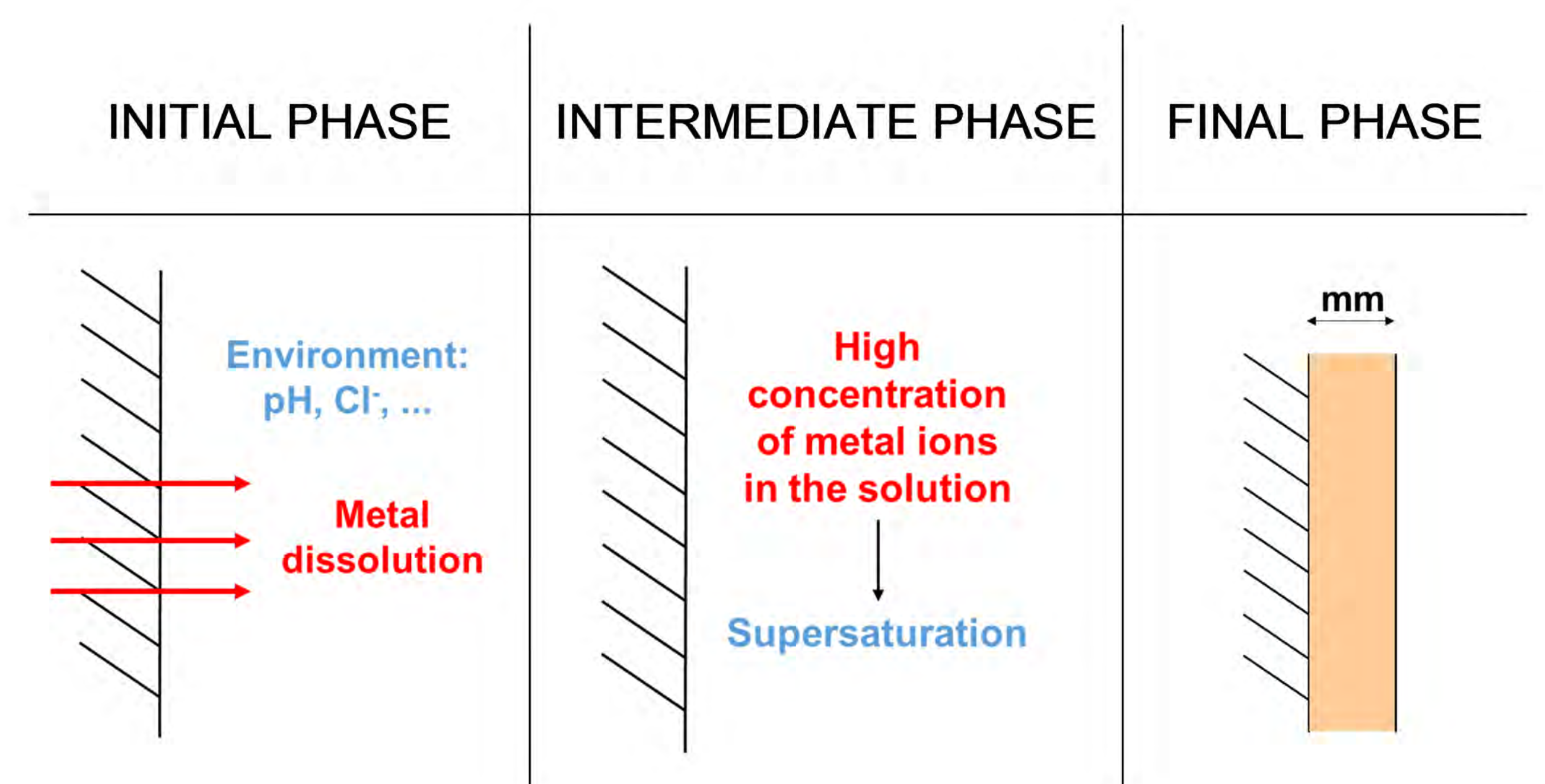
- How to completely prevent metallic materials degradation?
- How reactive is the fluid/material interface?
- What is the minimum  $[Cl^-]$  for pitting corrosion initiation?
- What is the influence of  $H_2S$  on corrosion?

## 4. Project Objectives

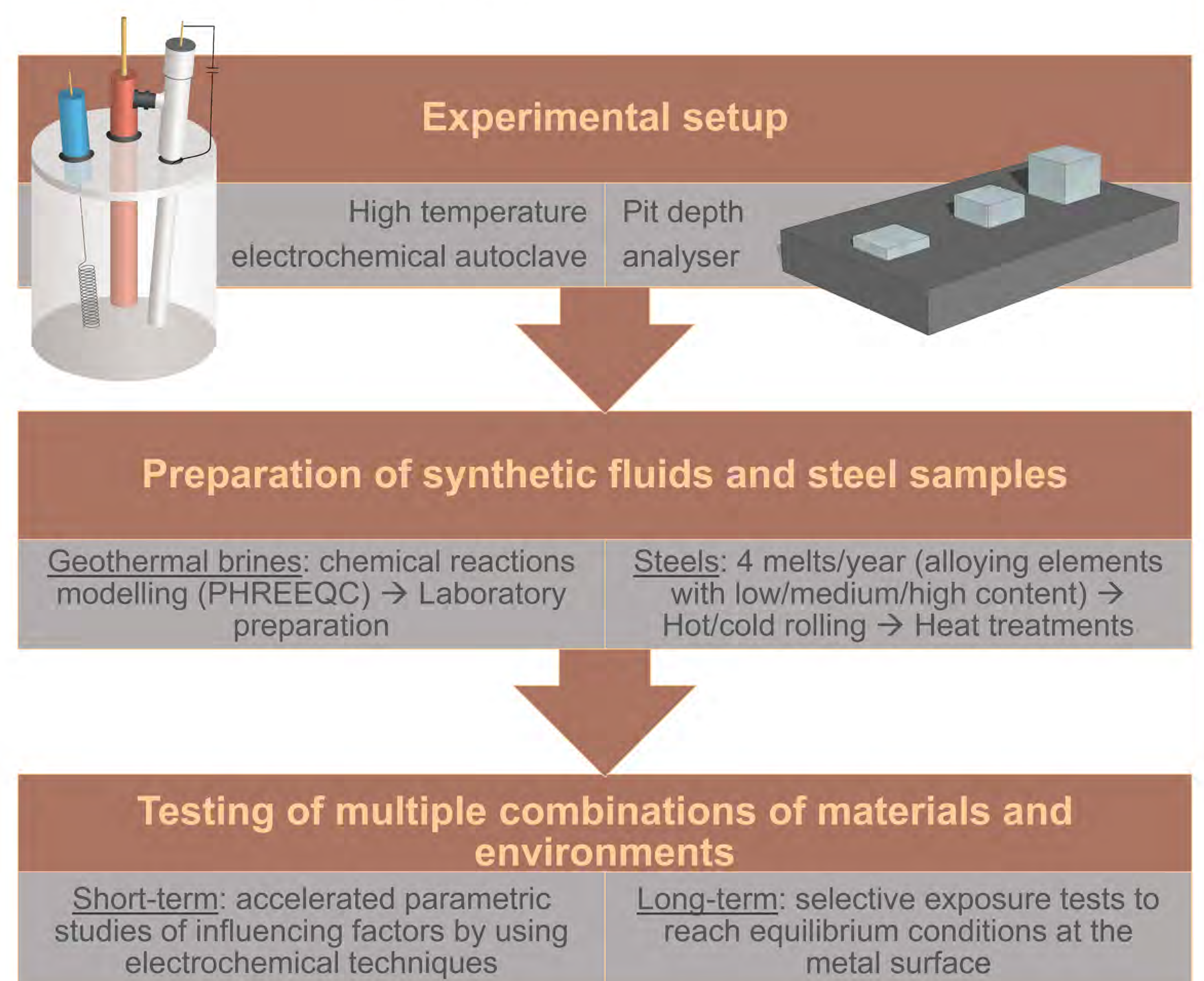
Based on the successful long-term experience of the low-alloyed carbon steel (Corten ® steel) at the atmosphere, the main goal is to develop tailor-made steels that:

- 1) contain metallic and/or non-metallic alloying elements,
- 2) form spontaneously a dense and adherent layer with the ions present in the aqueous solution,
- 3) and are protected against further corrosion.

Self-formation mechanism:



## 5. Experimental Approach



## 6. Conclusions

- In the last stages of the project, we will use natural geothermal brines to simulate real in-situ conditions.
- The project will contribute to build up a competence centre to conduct research on corrosion of materials and assist during the planning phase of deep geothermal power plants in Switzerland and abroad.
- In general, further research on corrosion and scaling is needed to make deep geothermal energy more accessible and economically attractive.

# Detecting Water through Electric Impedance Measurements

Gregory Emery, Alexandre Ganchninho,  
Joseph Moerschell

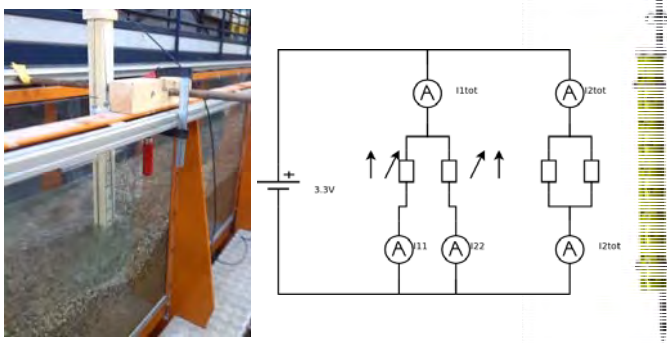
## 1. What is the problem ?

Environmental sensors are currently not well suited for deep water reservoir monitoring:

- limited depth of analysis with existing impedance sensors.
- inability to discriminate different components in measured impedance, in particular electrode double layer part.
- commercial equipment (e.g. for oil/gas reservoir exploration and monitoring) is not always adequate for water reservoir monitoring.

## 2. Discriminating water from sediments

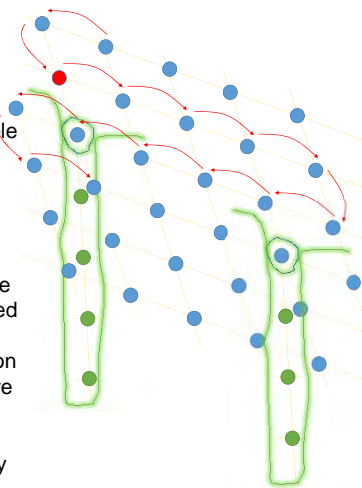
A novel limnimeter measuring water level and river bed sediment level through differential electric impedance sensing is used as starting point for the investigation.



- Water level and sediment level can be calculated from a double differential impedance measurement, independently of water and sediment conductivity.
- Alternatively, the water percentile per volume can be determined when the differential sensor is buried underground.
- But: technique limited to the length of the probe.

## 3. Network sensing concept

- Monitor geothermal water reservoir size, form and water flow.
- Network of surface and borehole electrodes.
- Single injection, multiple detection points, excitation frequency scan and spatial injection point scan.
- Phase lock-in detection scheme
- Correlate with natural or induced seismicity.
- Possibility for future combination with high resolution temperature and magnetic measurements.
- Differential measurements can be done in same way within dry boreholes as with limnimeter.



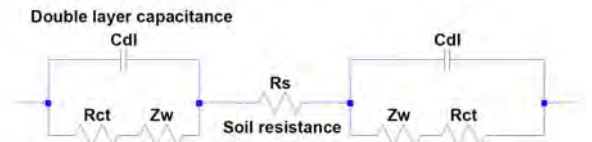
## 4. Laboratory test set-up for impedance analysis

Electric double layer around the electrodes represents a part of the total measured impedance which can be identified by frequency sweep of the excitation. This is first validated on small laboratory scale.



## 5. Equivalent model of soil impedance

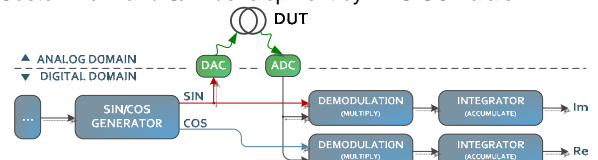
- Soil itself represents a resistance (ion transport), possibly in parallel with a capacitance (charge stored in the conducting channel).
- Electrode with double layer represented by capacitive and dissipative elements.
- Analysis based e.g. on Cole-Cole representation of impedance.
- Characteristic cut-off frequencies to be determined experimentally.



Charge transfer resistance Warburg element

## 6. Digital vector impedance analysis

- Digital excitation and synchronous demodulation.
- Frequency sweep range 1mHz...1MHz.
- Custom H/W and S/W development by HES-SO Valais.



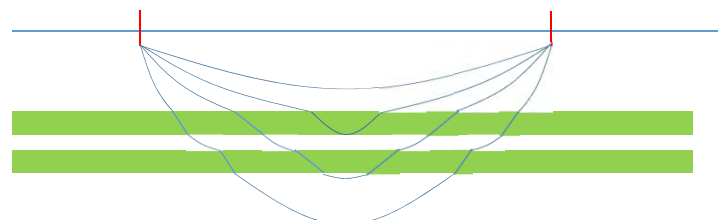
## 7. First field sensing tests

- Prototype electrode network for near surface underground placement.
- Asymmetric design to attenuate surface effects.
- Typical electrode spacing 1m...100m, 8 electrodes line, to be extended to 8 x 8 matrix.



## 8. Tomography

- Layer thickness defined by electrode spacing on surface.
- Successive layer analysis from ground to deeper layers.
- Adaptation of layer thickness to measured impedance values.



# Deep Borehole Seismometer

Charles Praplan, Christian Cachelin,  
Yves Ravedoni, Joseph Moerschell

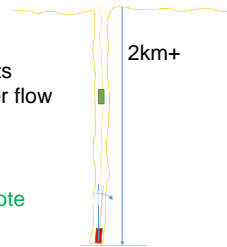
## 1. What is the problem ?

Environmental sensors are currently not well suited for DGE monitoring:

- scientific sensors are too costly or not available for deep boreholes.
- fracture motion detection puts particular requirements on sensors.
- commercial equipment (e.g. for oil/gas reservoir exploration and monitoring) is not always adequate for water reservoir monitoring.

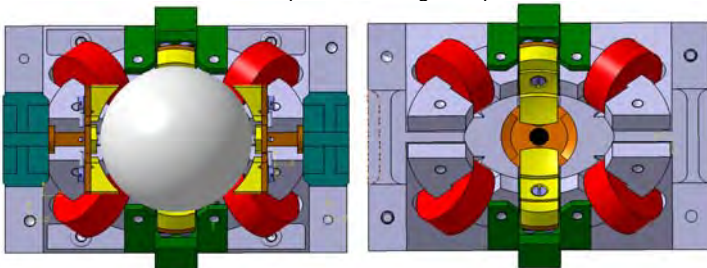
## 2. New deep borehole seismometer

- Monitor induced seismicity close to it's origin
- Performance target: sense microseismic events related to rock fracturing and pressurized water flow
- Extreme environment: 200bar+, 150°C, highly corrosive materials
- High temperature compatible sensor front end with acquisition electronics and higher-up remote driver/control/acquisition electronics (if borehole temperature >150°C)
- Ease of installation and orientation alignment
- Combination with dense low-cost accelerometer surface network



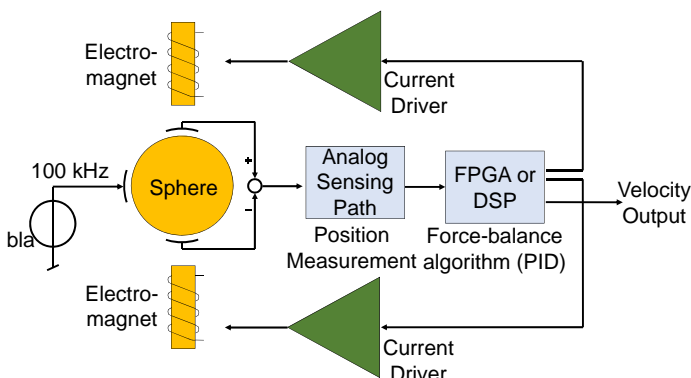
## 3. Sensor concept

- Magnetically suspended soft iron inertial sphere
- Capacitive displacement sensing in 3 dimensions, using 3 differential sensors and excitation signal injection to the sphere
- Centering actuation by 4 electromagnet pairs, replacing traditional spring suspension
- Choice of materials compatible with high temperatures



## 4. Digital force feedback circuit

The velocity output signal results from a feedback loop (one per axis) implemented in analog and digital circuits.



## 5. Laboratory test set-ups

Step-by-step build-up of the system, with 1dof and 2dof and then 3dof prototypes:



## 6. 3D sensor prototype

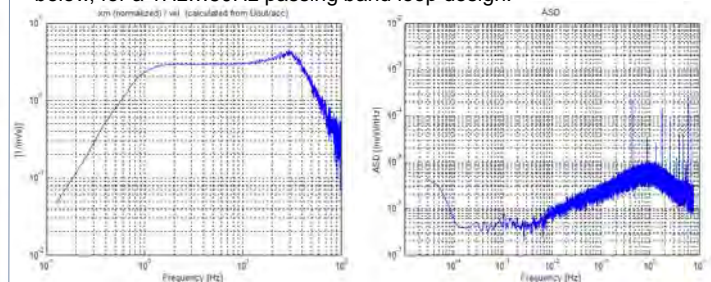
Benchtop model for validation of the principle of operation, model identification tests and development of feedback loops

3D



## 7. First performance measurements

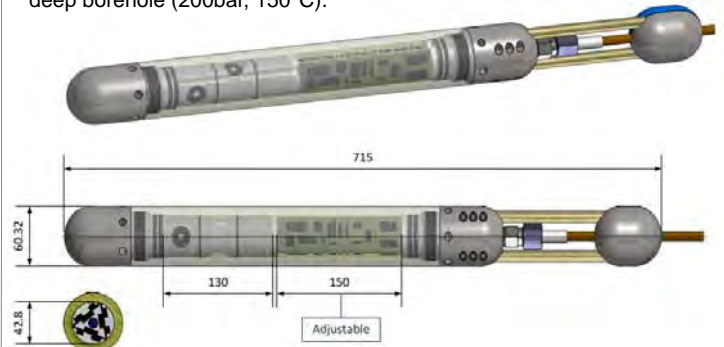
The 2D system was characterized. Its velocity output full scale range is  $\pm 0.157$ m/sec. Recorded transfer function and noise spectra are shown below, for a 1Hz...50Hz passing band loop design.



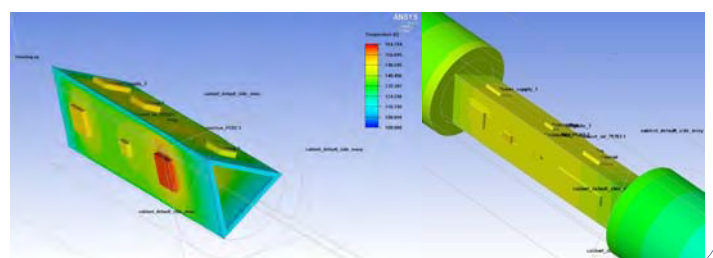
The passing band of the sensing loop can be modified, either to reduce the lower corner frequency, e.g. to 50mHz (already tested), or to increase the upper corner frequency, to e.g. 1kHz (to be tested).

## 8. Preliminary design for field test

First housing design to withstand high pressure and temperatures of deep borehole (200bar, 150°C).



The sensor cabinet can be adapted to classic geophone sensors, or to the new spherical sensor (larger diameter required). With this housing design, thermal simulations are done to determine heat flow from the electronics cabinet to the outside.



# Development of Numerical Tools for Heat Transfer Computations

David Roos, Lucian Hanimann, Luca Mangani, Ernesto Casartelli  
Hochschule Luzern, Technik & Architektur

## 1. Introduction

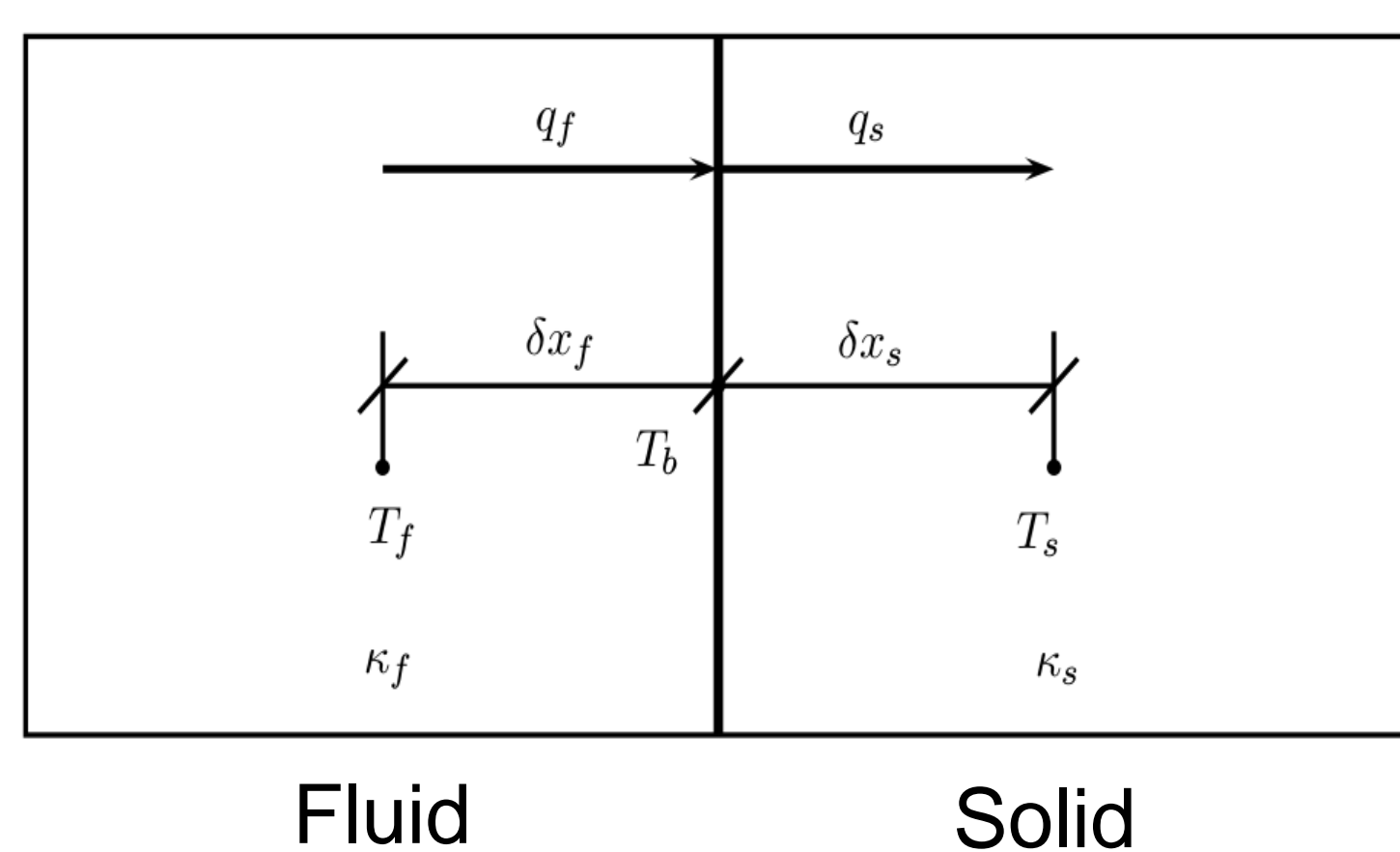
The main problems related to **pumps for geothermal applications** are the large thermal expansion of the device and the chemical composition of the pumped fluid. The thermal expansion, both in radial and axial direction, leads to large changes in the relative position between runner and casing. These changes affect the fluid dynamics of the pump, the forces acting on it (bearings, rotor dynamics) and the matching between runner and diffuser, therefore influencing the overall pump characteristic including efficiency and stability. In order to investigate these effects, conjugate heat transfer simulations, where solids and fluids are computed simultaneously, need to be applied to predict the temperature distribution in the pump components. Current implementations in open-source as well as commercial software are often inadequate, especially where turbulence models and wall functions are concerned. The goal of this work is to develop and validate tools for the reliable RANS (Reynolds-averaged Navier-Stokes) and LES (Large Eddy) simulation of conjugate heat transfer applications in geothermal pumps.

## 2. Activities

- Investigation of Conjugate Heat Transfer (CHT) capabilities of commercial and open-source software (OpenFOAM)
- Development of mesh-independent models for CHT (wall functions)
- Improvement of the numerical performance of CHT computations
- Investigation of turbulence models for CHT applications and validation
- Development of an incompressible LES solver for OpenFOAM with heat transfer capabilities

## 3. Conjugate Heat Transfer Improvements

The interface boundary contributions between fluid and solid domains are discretised implicitly and the coupling boundary conditions are updated during the inner iterations. Both these measures lead to a significant improvement in stability for CHT simulations.



$$\dot{q}_s = \dot{q}_f$$

$$\kappa_f \frac{T_b - T_f}{\delta x_f} = \kappa_s \frac{T_s - T_b}{\delta x_s}$$

$$T_b = \frac{\kappa_s \delta x_f}{\kappa_f \delta x_s + \kappa_s \delta x_f} T_s + \frac{\kappa_f \delta x_s}{\kappa_f \delta x_s + \kappa_s \delta x_f} T_f$$

Fig. 1: Boundary condition (source) + implicit contributions

The performance for steady-state computations has been greatly increased (speed-up of more than one order of magnitude) due to the introduction of separate implicit relaxation factors for solid and fluid domains respectively.

$$\underline{L} \cdot \underline{x} + \frac{D}{\alpha} \cdot \underline{x} + \underline{U} \cdot \underline{x} = \underline{b} + \frac{D}{\alpha} \cdot \left(\frac{1}{\alpha} - 1\right) \cdot \underline{x}$$

## 3. Conjugate Heat Transfer Improvements (cont.)

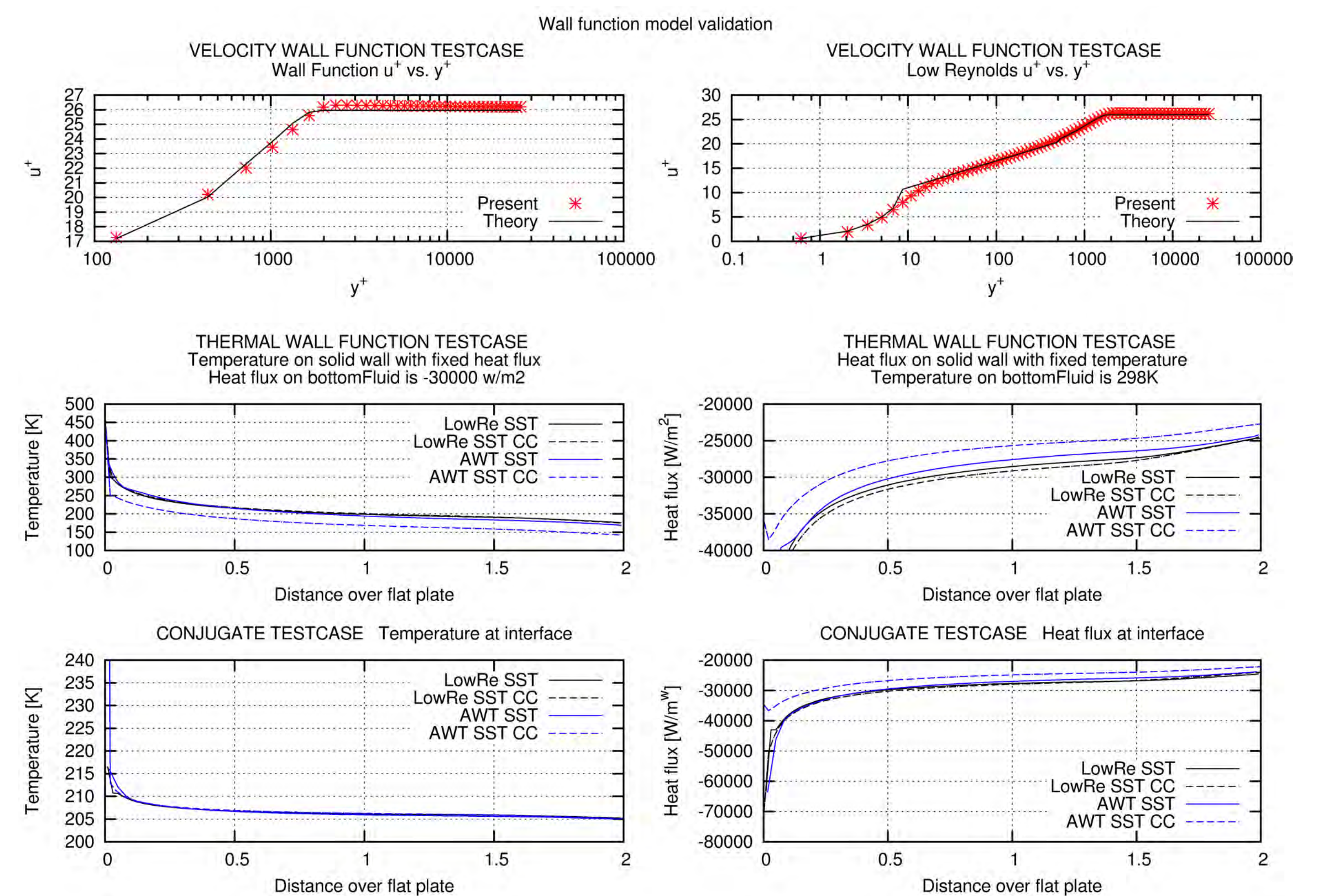


Fig. 2: Flat plate test case with and without conjugate heat transfer. The results labeled «CC» were obtained using a commercial code. The «AWT» label indicates the use of wall functions.

## 4. Large Eddy Simulation with Heat Transfer

An explicit solver for large eddy simulation based on the projection method was implemented in OpenFOAM. It was verified and validated along with a selection of existing and newly implemented LES turbulence models. It has shown to be highly accurate in cases where Reynolds-averaged turbulence modelling (RANS) approaches failed to predict useful results.



Fig. 3: Averaged streamlines behind turbulator

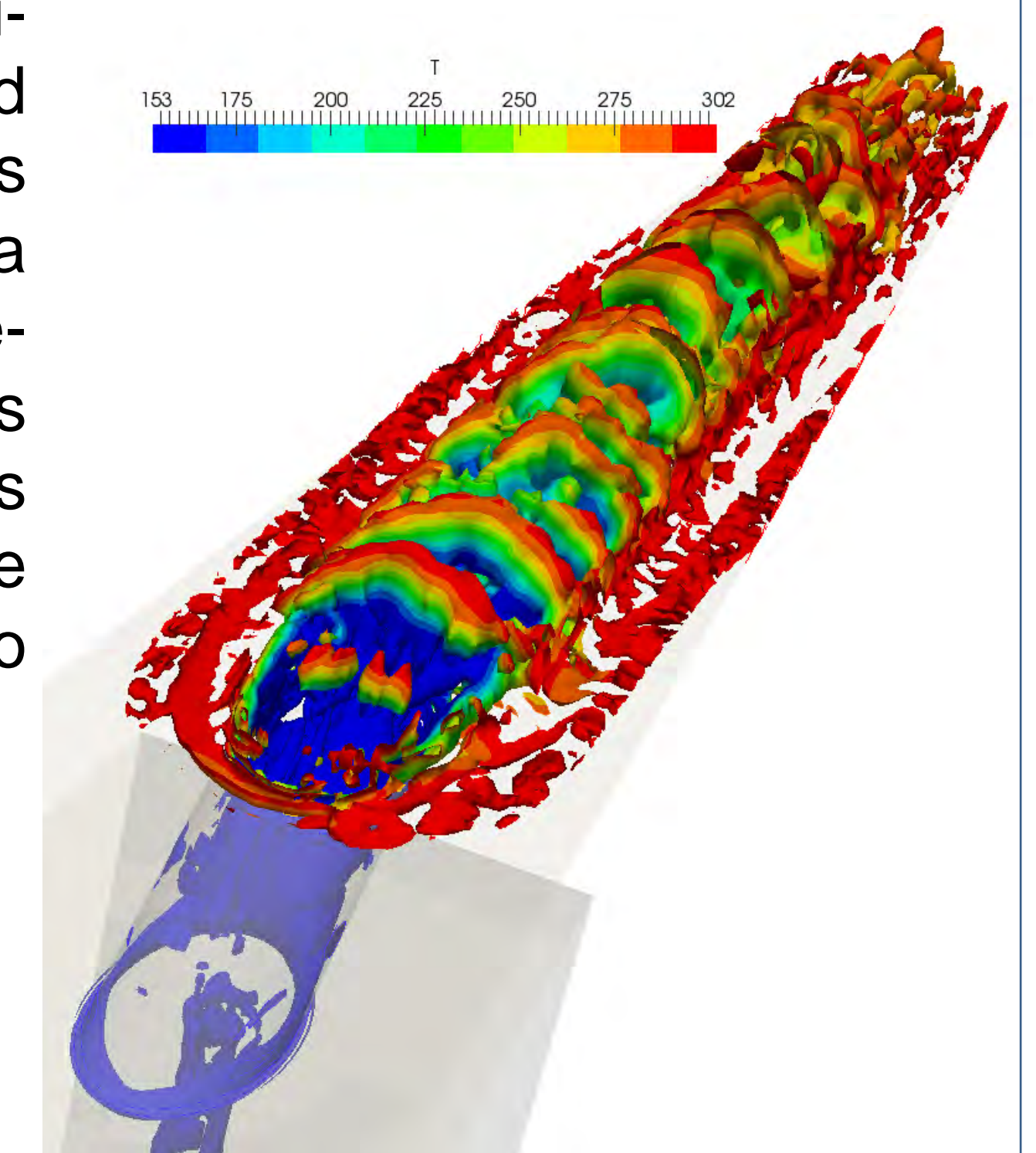


Fig. 4: Turbulent structures of a cooling jet in crossflow at low blowing rate

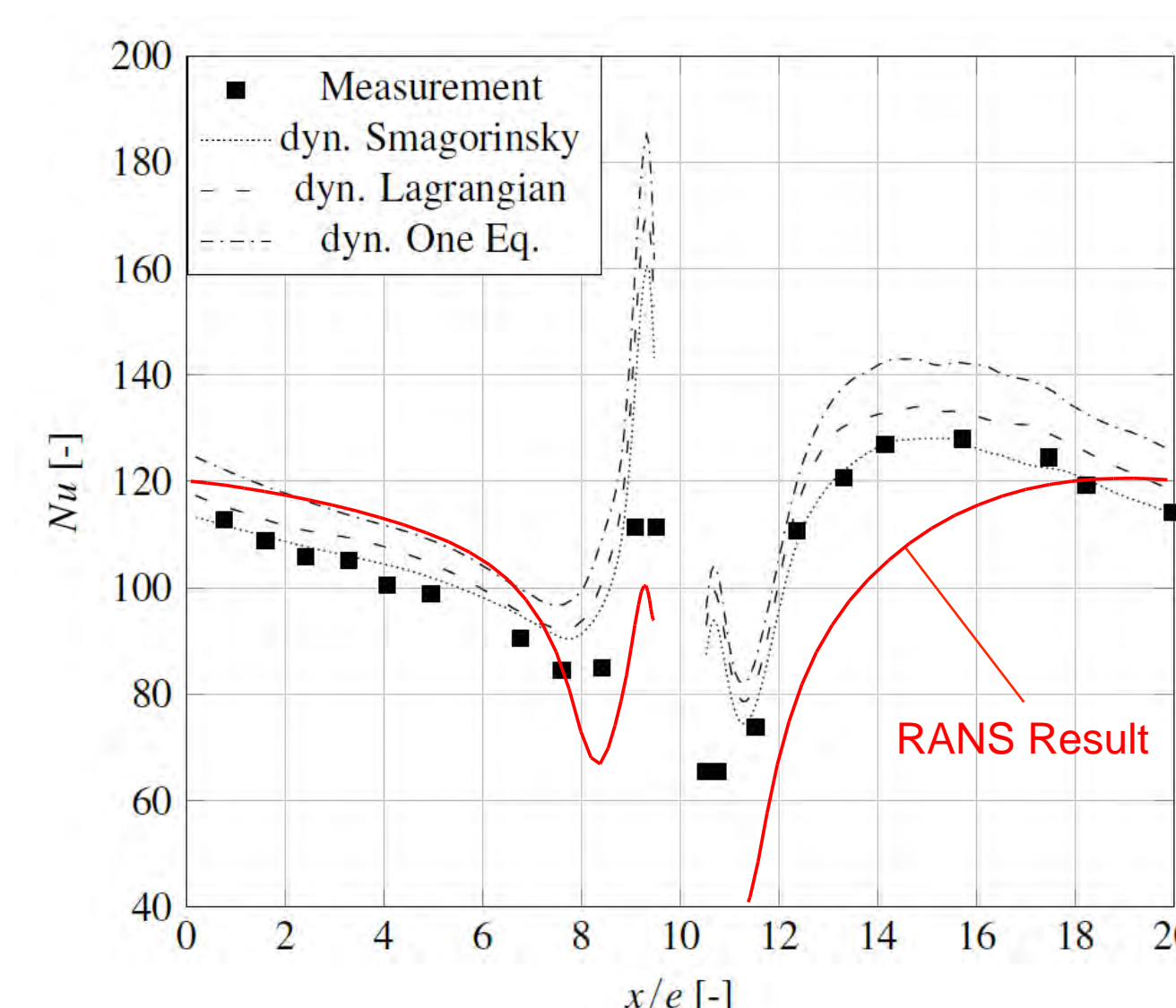


Fig. 5: Nusselt number distribution over turbulator for different LES models

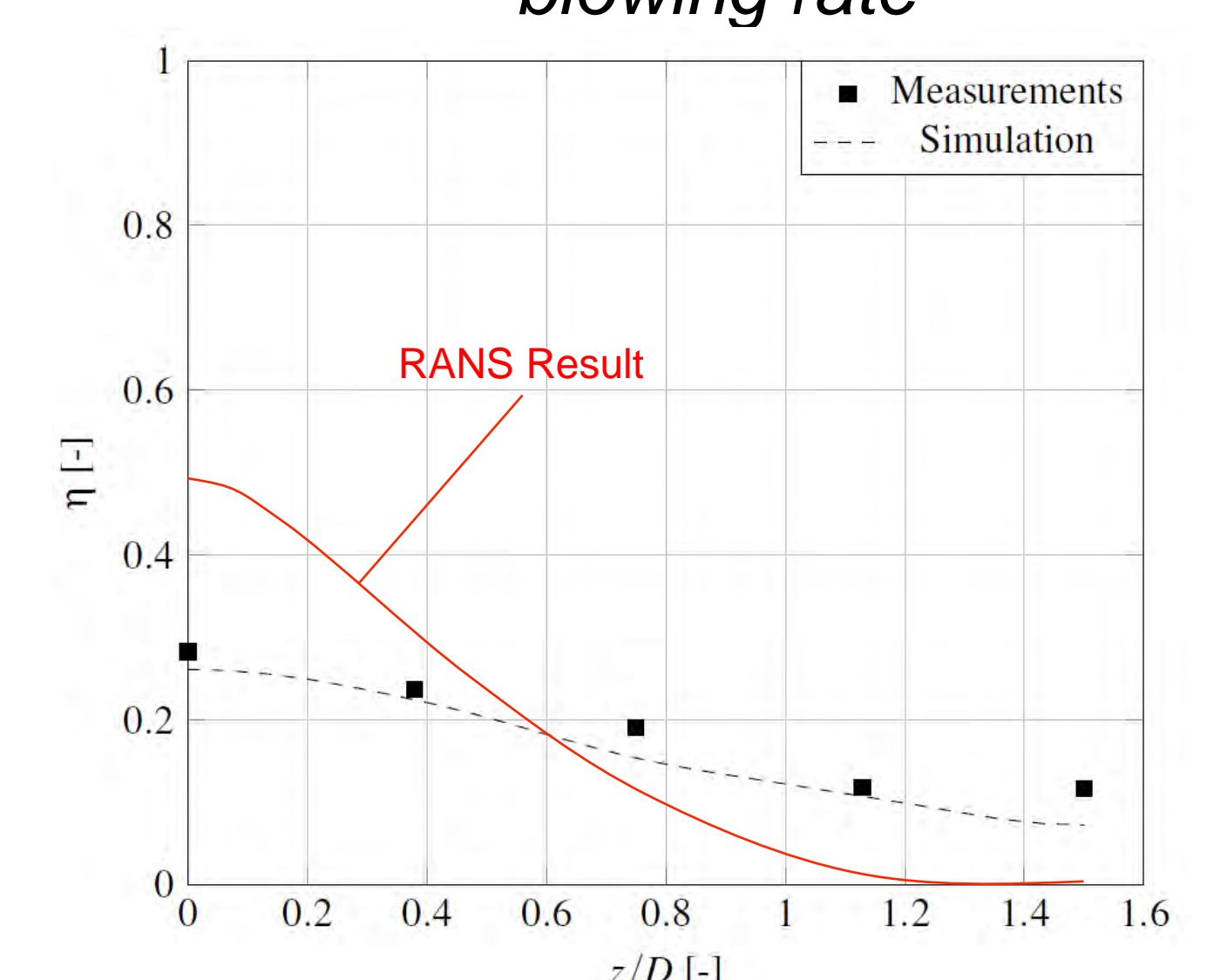


Fig. 6: Lateral cooling effectiveness of jet in crossflow

## 5. Conclusions

The conjugate heat transfer method was successfully implemented in OpenFOAM. Fluid and thermal wall functions were implemented and validated. Significant improvement for modelled quantities at the walls could be obtained, providing the basis for accurate coupling of the fluid and solid components. The LES solver was verified and validated, allowing the possibility to combine the two techniques for highly accurate temperature predictions.

# Analytical solution of the power production of a deep coaxial heat exchanger

R. Schnellmann, P. Hardegger, H.R. Schneider  
University of Applied Sciences Rapperswil (HSR)

## 1. Introduction

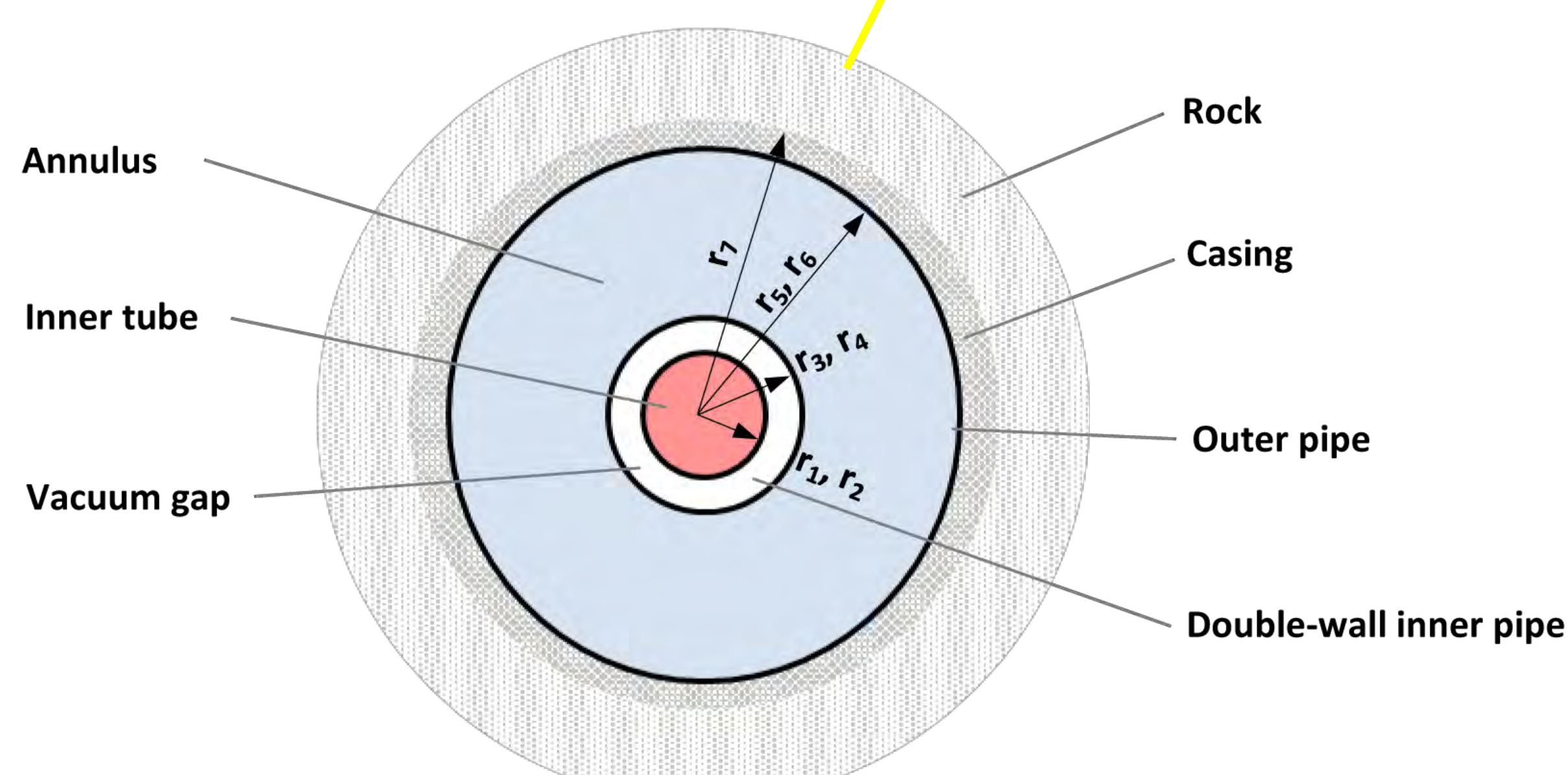
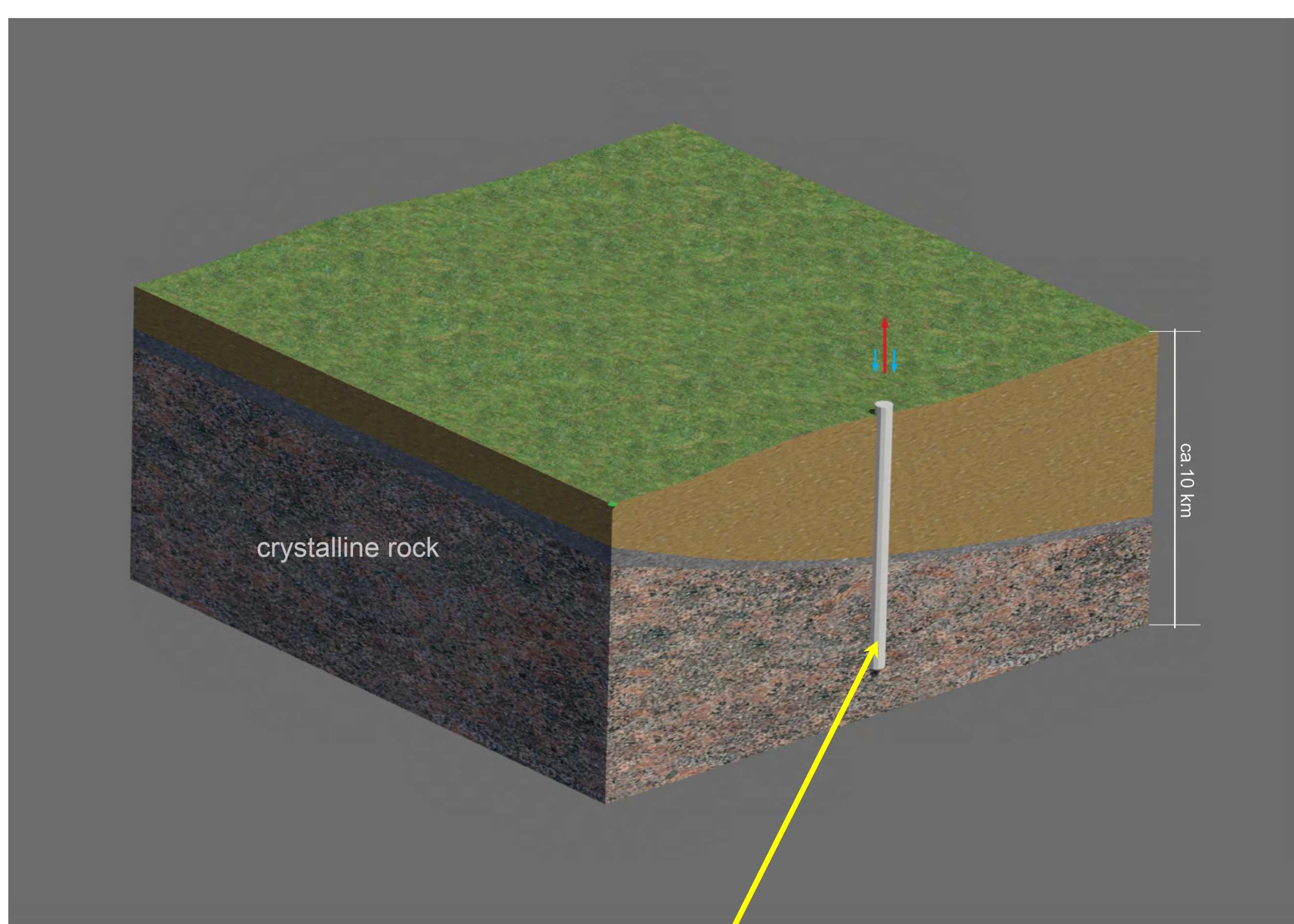
An analytical solution of the geothermal power generated by a single closed loop coaxial heat exchanger is presented.

The heat exchanger consists of an outer pipe and an inner double-wall pipe appropriately insulated with circulating fluid pumped into the annulus of the coaxial heat exchanger. Due to the heat of the surrounding rock mass, the fluid in the annulus is heated as it flows to the base of the coaxial heat exchanger where it changes direction and flows upwards via the inner production pipe. At the ground surface the heated fluid is converted into electrical energy. Due to the thermal power produced, the temperature field in the rock mass around the vertical borehole is radially affected.

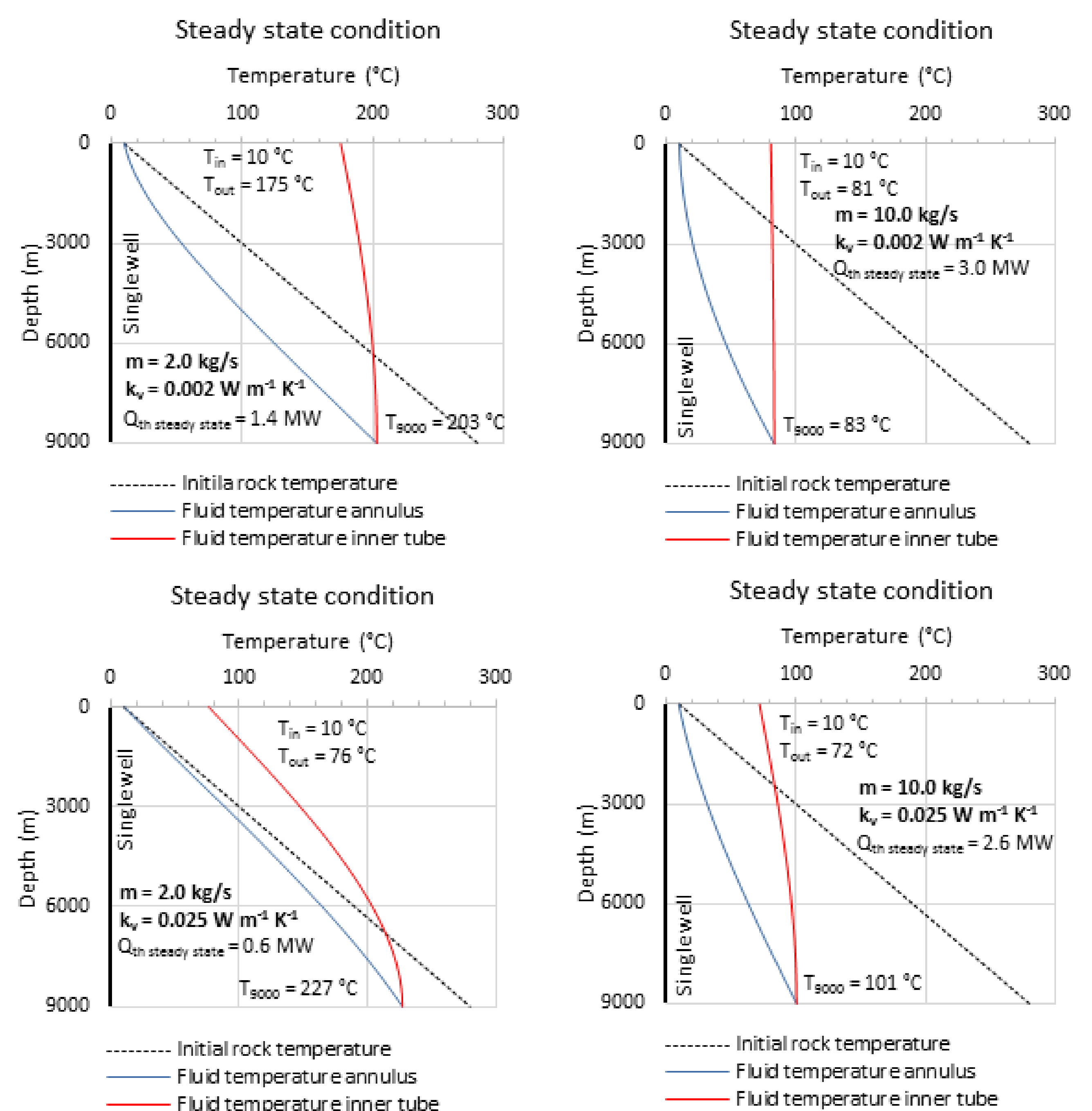
In addition to the geothermal power produced by a deep single borehole, the temperature profiles in the annulus and the inner tube of the coaxial heat exchanger as well as the temperature profile in the adjacent rock mass due are of interest. In order to understand the behavior of the coaxial heat exchanger system with the main controlling variables a coupled steady-state analytical solution has been worked out.

A crucial point in the method presented above is the successful, fast and cheap execution of a stable cylindrical borehole down to depths of 8 – 10 km. Pioneering high pressure - high temperature triaxial strength tests on rock samples will be carried to develop 3-D failure criteria for a comprehensive assessment of borehole stability down to 8- 10 km. The specialized testing equipment is under construction and will be ready for initial experiments by the end of this year.

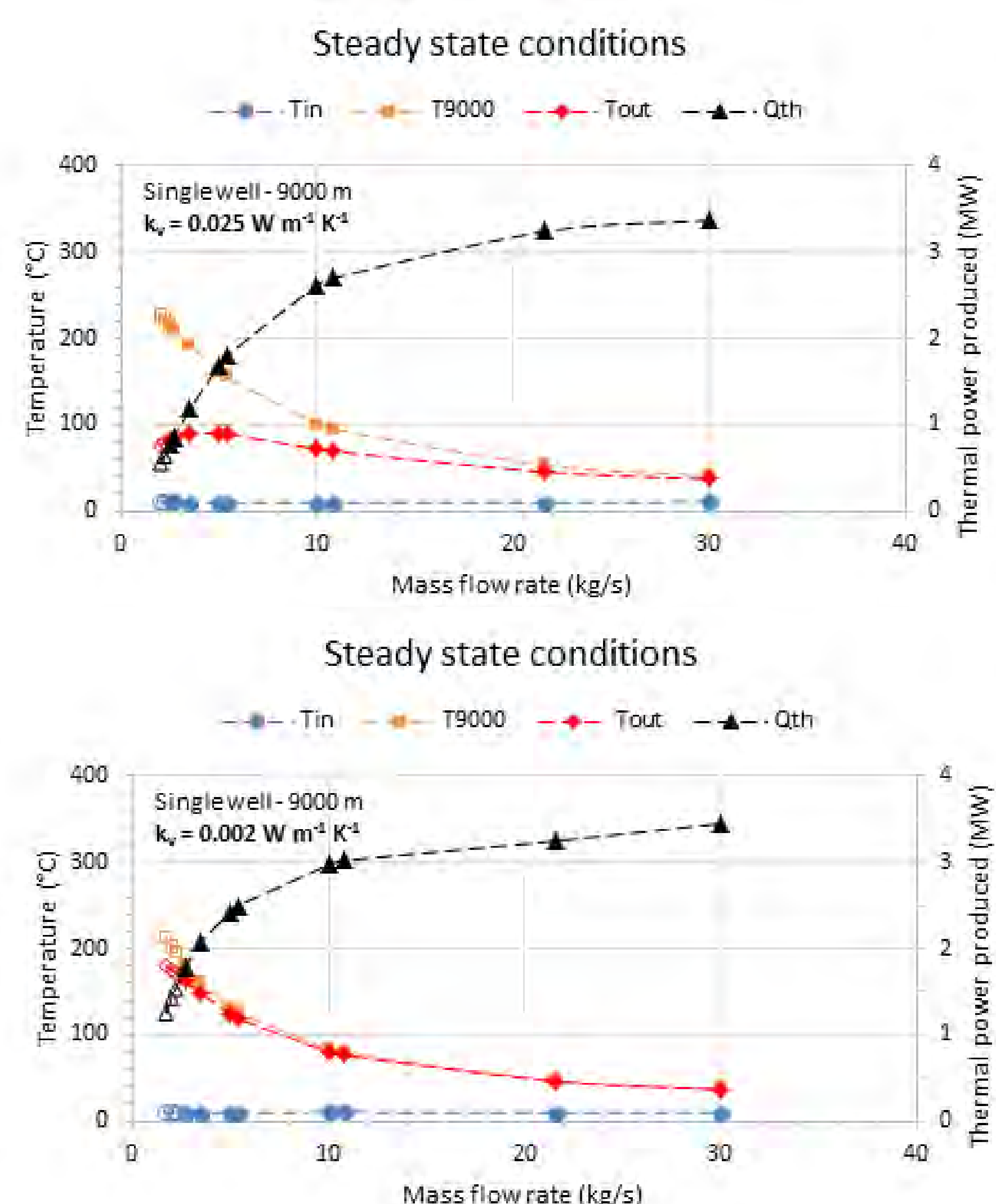
## 2. Geothermal System Overview



## 3. Typical results of the coupled steady-state analyses



The results are shown for two mass flow rates  $m$  of the circulating fluid and for two different thermal conductivities  $k_v$  of the double-wall pipe. The thermal power produced at steady state  $Q_{th}$  is given in the graphs above.



The two summarizing graphs on the left show the inlet temperature at the ground surface  $T_{in}$  (blue), the temperature of the circulating fluid at the base  $T_{9000}$  (orange), the outlet temperature at the surface  $T_{out}$  (red) and thermal power produced  $Q_{th}$  (black).

## 4. Conclusions

The thermal power production of a single, vertical coaxial heat exchanger extending down to 9000 m into crystalline bedrock has been evaluated. The steady state coupled heat-fluid-analysis have been presented. Higher thermal power produced results also in a larger radius of influence of cooling in the adjacent crystalline rock mass. For the steady state analyses carried out, the radius of influence of cooling the surrounding rock mass was less than 150 m.

# Impact of polymers in oil-well cementing for geothermal wells

M. Palacios, R. K. Mishra, D. Sanz-Pont, R. J. Flatt\*

## 1. Introduction

The cementing of geothermal wells supports mechanically the metallic well casing pipes and it mitigates their corrosion. However, the high temperatures and pressures encountered in deep wells involve many technological challenges such as poor rheological properties and quick setting of cement slurries. On site, a combination of different chemical admixtures including dispersants, set retarders and accelerators are normally used although a loss of performance is often found.

In the Group of Physical Chemistry of Building Materials, in the frame of WP3 Task 3.1 "Geo-energy technologies", we investigate the role of polymers on cement hydration kinetics and rheological properties of cement slurries at the extreme conditions encountered in geothermal well. This will be done using an experimental and molecular modeling approach.

## 2. Methods

- **Isothermal calorimetry** to study the impact of polymer structure and dosage on cement reaction kinetics with the temperature.
- **High-end rheometer** to investigate the rheological properties of the superplasticized retarded mixes.
- **Molecular modeling** to understand the impact of aluminate ions as well as organic admixtures during tricalcium silicate,  $C_3S$  (major constituent of cement clinker) hydration.

## 3. Highlights of the project

For first time, it has been found that it is possible to delay cement hydration as the temperature increases by using specific dosages and structures of comb-copolymer dispersants. This retardation increases with the increase of the charge density of the polymers and in presence of supplementary cementitious materials (SCMs). In particular, it is possible to delay cement hydration up to 100 hours at 70 °C with respect to 23 °C (Figure 1). The passivation of silicates hydration by the aluminum in solution probably explains this surprising effect; as the concentration of aluminum increases with the dosage of admixture and with the temperature in cements containing SCMs.

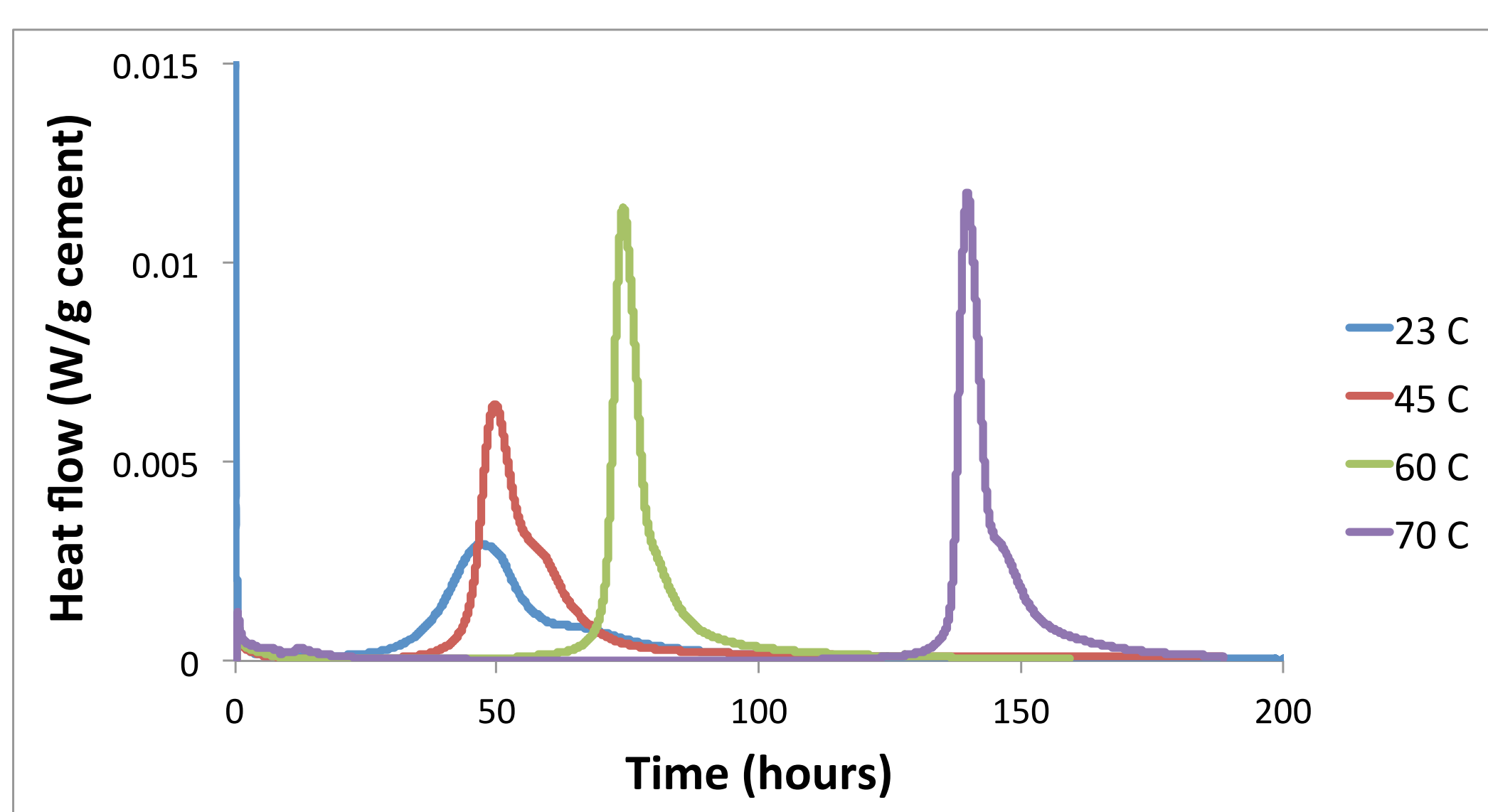


Figure 1. Calorimetry curves at different temperatures of cement pastes in presence of a specific comb-copolymer

The addition of specific polymers, also decreases the maximum rate and the slope of the acceleration period with temperature with respect to non-admixed systems (Figure 2). This would slow down cement hydration after it starts rather than just delay the onset.

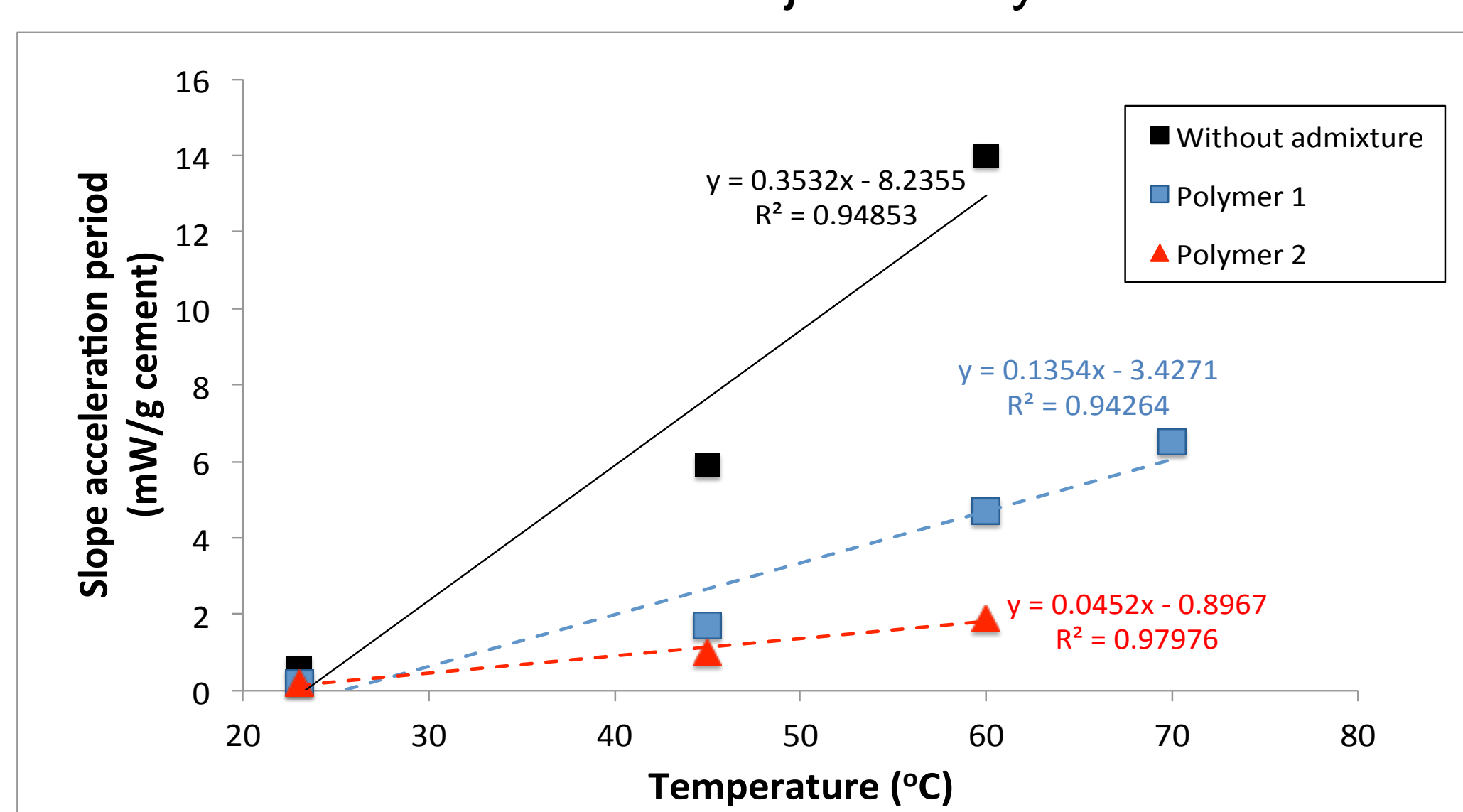


Figure 2. Slope of the acceleration period of cement pastes at different temperatures

The mechanisms behind molecular interactions between  $C_3S$  and aluminate ions has also been studied by molecular dynamics (MD) simulations using all-atom accurate force field models. Different types of possible hydroxylated  $C_3S$  (hyd.  $C_3S$ ) surfaces are shown below at different pH values (Figure 3).

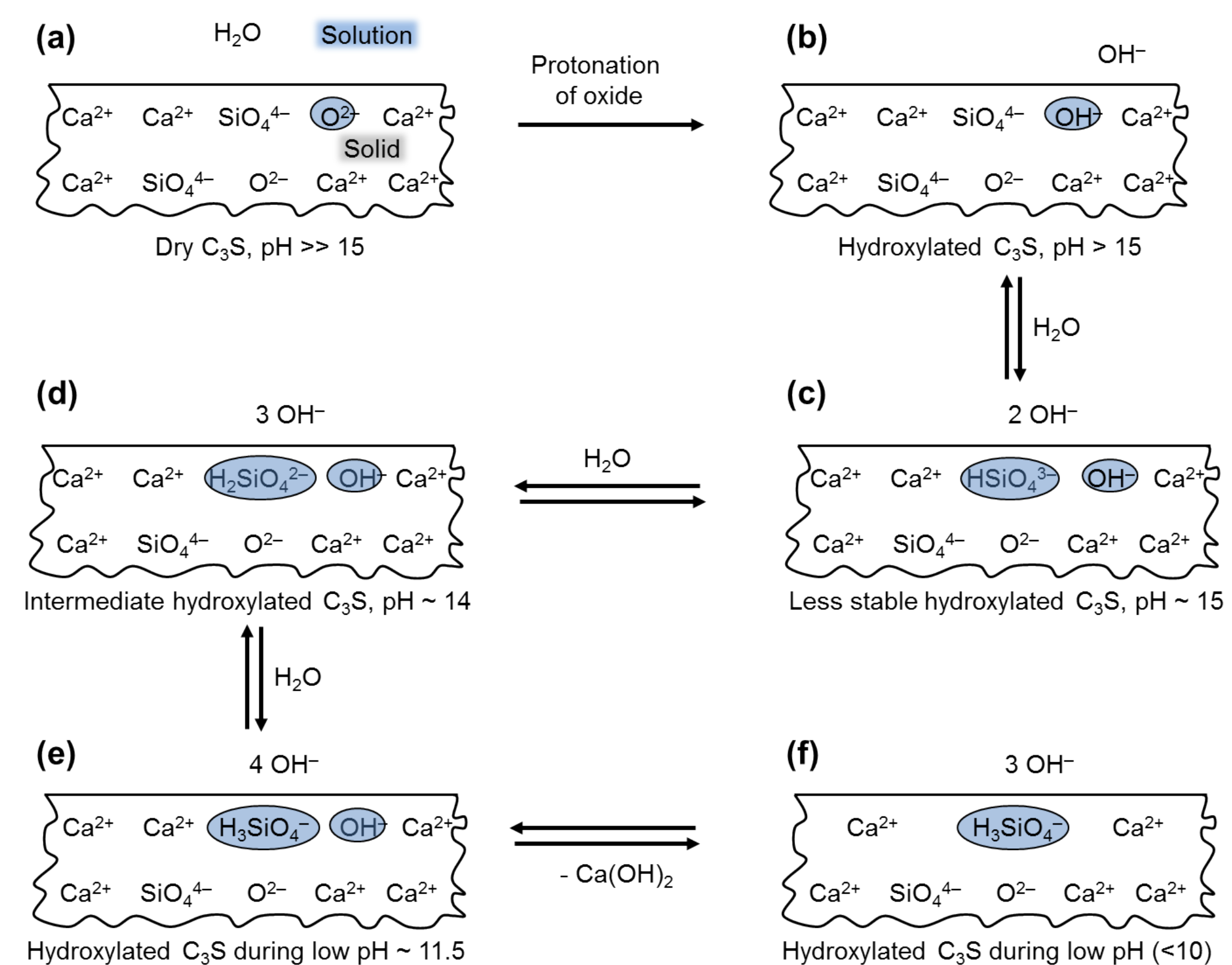


Figure 3. Schematic of different possible steps of dissolution of  $C_3S$  which involves hydration of superficial oxide ions as well as formation of silanol groups.

Molecular model of hydroxylated  $C_3S$  surfaces were validated by computing interfacial energy with water using validated force field parameters (Table 1). Using MD simulations, we also computed interactions of aluminate ions on the hyd.  $C_3S$  surface.

Table 1. Interfacial energy of different types of hydroxylated  $C_3S$  surfaces (described in Figure 3) with water using molecular dynamics simulations.

Types of $C_3S$ Surface	Interfacial Energy, $mJ/m^2$	pH	Temperature, K
Dry $C_3S$ (step a)	$450 \pm 35$	$\gg 15$	298
Hyd. $C_3S$ (step b)	$-267 \pm 28$	$> 15$	298
Hyd. $C_3S$ (step c)	$-386 \pm 30$	$\sim 15$	298
Hyd. $C_3S$ (step d)	$-516 \pm 35$	$\sim 14$	298
Hyd. $C_3S$ (step e)	$-713 \pm 50$	$\sim 11.5$	298

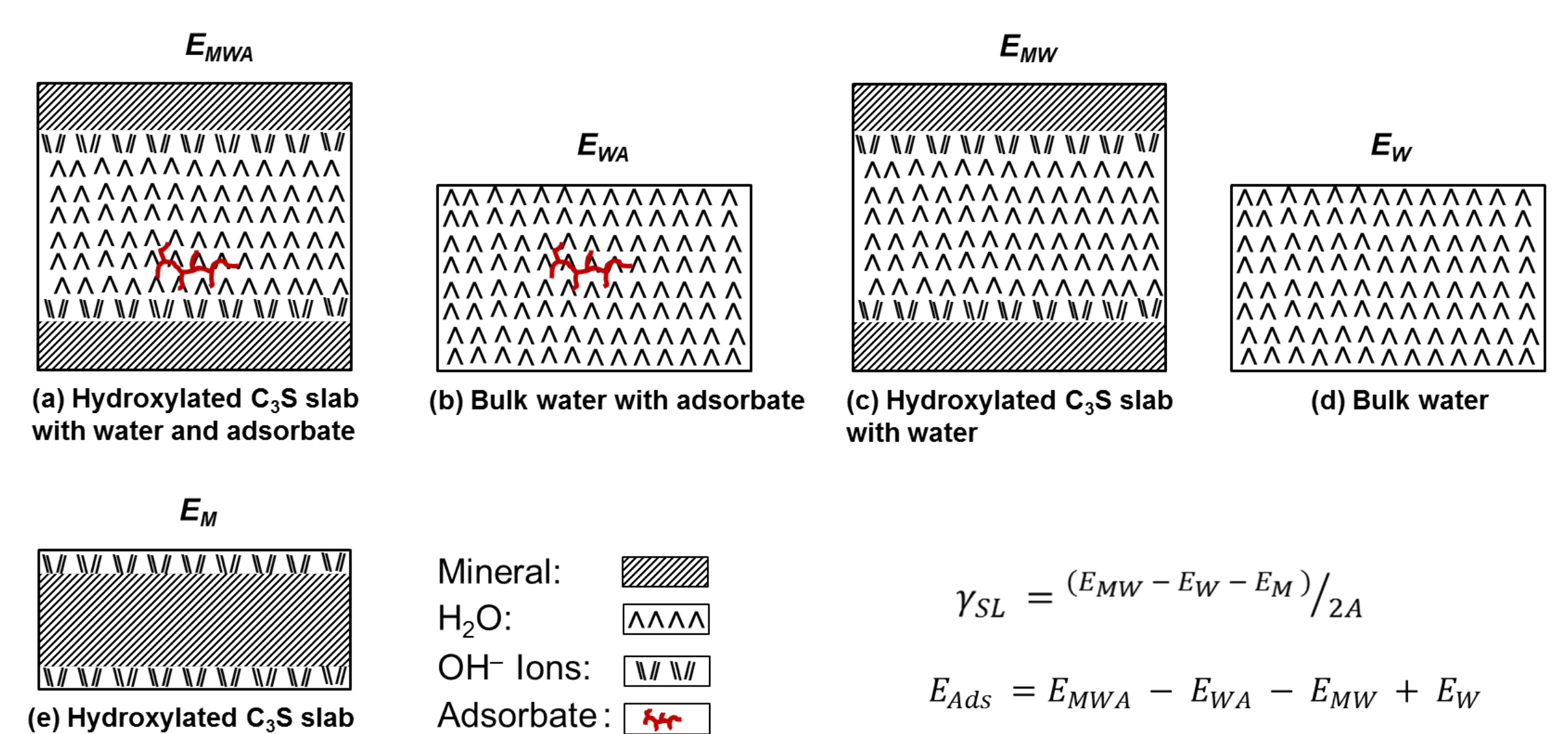


Figure 4. Schematic of the calculations of solid-liquid interfacial energy  $\gamma_{SL}$  and adsorption energy  $E_{Ads}$  using molecular dynamics simulations.

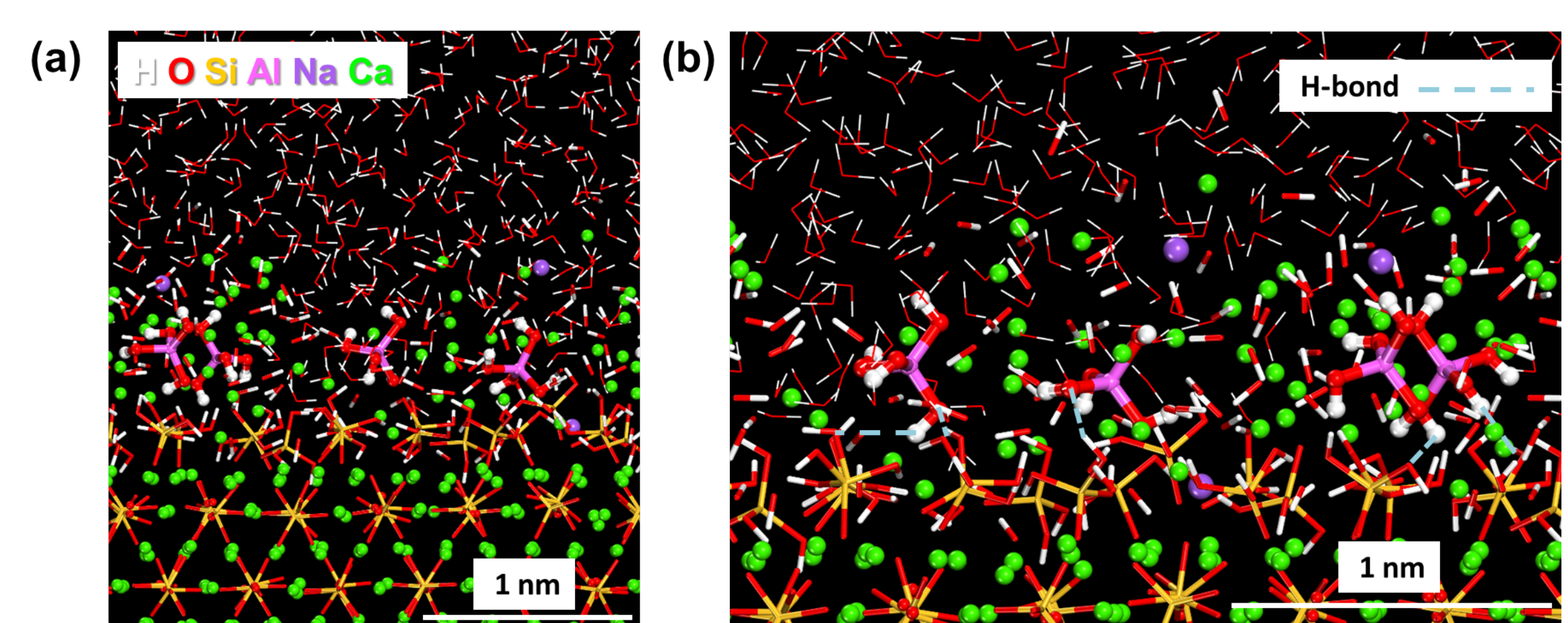


Figure 5. Interactions of aluminate ions with hyd.  $C_3S$  (a) Hyd.  $C_3S$  (formation of  $SiO(OH)_3^{1-} + H_2O + NaAl(OH)_4$ ), (b) Formation of hydrogen bonds between  $Si-O \cdots HO-Al$  or  $Si-OH \cdots O-Al$ .

## 4. Future research

The following studies at high temperature will be done:

- Rheological properties of the superplasticized retarded mixes.
- Impact of organic admixtures in presence of aluminates by molecular modeling.

\*Contact information: Prof. Robert J. Flatt, Institute for Building materials, ETH Zurich, Switzerland. E-mail: flatt@ethz.ch